PONTIFICIA UNIVERSIDAD CATOLICA DE CHILE
SCHOOL OF ENGINEERING

UNCERTAINTY QUANTIFICATION FOR MULTIGROUP NEUTRON DIFFUSION EQUATIONS USING SPARSE TENSOR APPROXIMATIONS

MARÍA CONSUELO FUENZALIDA

Thesis submitted to the Office of Research and Graduate Studies
in partial fulfillment of the requirements for the degree of
Master of Science in Engineering

Advisor:
CARLOS JEREZ

Santiago de Chile, April 2018

PONTIFICIA UNIVERSIDAD CATOLICA DE CHILE
SCHOOL OF ENGINEERING

UNCERTAINTY QUANTIFICATION FOR MULTIGROUP NEUTRON DIFFUSION EQUATIONS USING SPARSE TENSOR APPROXIMATIONS

MARÍA CONSUELO FUENZALIDA

Members of the Committee:
CARLOS JEREZ
ELWIN VAN'WOUT
RYAN MCCLARREN
JOSÉ LUIS ALMAZÁN

Thesis submitted to the Office of Research and Graduate Studies
in partial fulfillment of the requirements for the degree of
Master of Science in Engineering

Santiago de Chile, April 2018

ACKNOWLEDGEMENTS

First of all, I would like to thank Pontificia Universidad Católica de Chile for giving me the chance of living an enriching university experience. This six years of undergraduate and postgraduate studies, which concludes today with my master's thesis defense, allowed me to develop my skills and knowledge, to broaden my world view and to meet wonderful people. I will remember this stage of my life longingly and with affection.

Thanks to my advisor, Carlos Jerez, whom I was able to live many research experiences since my third year of college. He showed me the way of contribution to the world through knowledge creation. I appreciate he trusted in my abilities maybe more than me.

Thanks to all those professors who, through an outstanding teaching, they awakened my passion for math and science during my college years (JL). Thanks to my fellows who offered me an indispensable support in many difficult courses (DM, JG, FF) and to my office mates who offered me a continuous help and encouraged me to persevere (JP, RA).

Thanks to Seed Fund TAMU-PUC Corfo 2030 and Fondecyt Regular 1171491 for funding this project, specifically, for giving me the chance of doing a research internship in Texas A&M to start developing my thesis topic. Thanks to all the people who generously encouraged me to accept this challenge (CJ, MV). Thanks to professor Ryan McClarren for guiding my research there and to the good friends I made in that country.

Thanks to my family and friends, who accompanied me in this process in many ways. They helped me to develop myself integrally and they assisted me to overcame the difficult moments every research activity entails at times.

Lastly, I am thankful to God, for He has gave me the chance of developing my talents and translating them into projects such as this thesis. I ask him to guide me on how to use my skills to be a positive contribution to the world.

TABLE OF CONTENTS

LIST OF FIGURES

LIST OF TABLES

ABSTRACT

We develop a novel method to compute first and second order statistical moments of neutron flux inside a reactor by solving the multigroup diffusion equation. Randomness comes from the lack of precise of knowledge of external sources as well as of cross-section parameters. Thus, the flux is itself a random variable. As Monte-Carlo simulations entail intense computational work, we are interested in deterministic approaches. By assuming as given both the second moment of sources and probability distributions of cross-section parameters, we present an efficient method based on a Sparse Tensor finite-element method approximation as well as the use of Smolyak quadratures. Numerical experiments are provided to validate our claims and further research lines drawn.

Keywords: Sparse Tensor Approximation, Multigroup Diffusion Equation, Uncertainty Quantification, Smolyak Quadrature.

RESUMEN

En esta tesis se desarrolla un método para calcular el primer y segundo momento del flujo de neutrones dentro de un sistema nuclear resolviendo una ecuación de difusión sin dependencia en el tiempo. La aleatoriedad proviene principalmente de la falta de conocimiento acerca de la fuente externa y de los parámetros conocidos como secciones transversales. Como el flujo depende de la fuente y los parámetros, es también una variable aleatoria. Como las simulaciones de Monte-Carlo tienen un alto costo computacional, se opta por enfoques determinísticos para resolver el problema. Asumiendo como dados el primer y segundo momento de la fuente y la distribución de los parámetros, se presenta un método eficiente basado en el método de elementos finitos con aproximaciones ralas y en el uso de cuadraturas de Smolyak. Se presentan experimentos numéricos y futuros temas a desarrollar.

Palabras Claves: Aproximaciones Tensoriales Ralas, Ecuación de Difusión con múltiples grupos, Cuantificación de Incertidumbre, Cuadraturas de Smolyak.

1. INTRODUCTION

The general problem of particle transport can be applied to a variety of situations from rarefied gas dynamics for aircraft in the upper atmosphere, to charged particle transport in space environments, as well as nuclear reactions in energy systems (McClarren, 2017) and radiative transfer in the atmosphere (Myneni, Radiative, , & 1993, 1993). While there are a number of developed techniques for solving these problems, the question of how uncertainties in the simulation inputs affect the predictions remains a challenging task both numerically and theoretically (McClarren, Ryu, & Drake, 2010; McClarren & Wohlbier, 2010; McClarren, Drake, Morel, & Holloway, 2010; Hauck & McClarren, 2013; Hanuš & McClarren, 2016).

We aim to tackle high-dimensional uncertainties in particle transport problems by considering steady-state multigroup diffusion equations. This model is widely used in nuclear reactor theory for solving the phase-space distribution of neutrons in a system where neutron-nucleus reactions occur, despite its limitations for specific physical situations (Saracco, Dulla, & Ravetto, 2012; Lamarsh, 2001). Of particular interest for nuclear engineers is the eigenvalue problem of computing the neutron fission chain reaction, or so-called criticality parameters, for which first existence theorems were provided by Habetler and Martino (Habetler & Martino, 1961), and numerous computational schemes have been developed (Haidar, 1992; Sanchez & McCormick, 1982; Hosseini & Saadatian-Derakhshandeh, 2015). Numerically, the criticality problem is an eigenvalue problem that can be solved via the standard Finite Element Method (FEM) built over general triangular meshes (Hasan & Conn, 1987; Wang & Ragusa, 2009). Based on this computational method, we will provide an efficient way to compute statistical moments for solutions subject to uncertainty in (i) *sources* and (ii) *cross-section parameters*. Nonetheless, we will not address the associated eigenvalue problem. Rather we focus on the forward problem where we solve for the distribution of neutrons given a source. Such problems are important in radiation protection/shielding and nuclear hydrocarbon exploration/production.

The standard method of choice for operator equations with uncertain input data subject to noisy observation data is the Monte Carlo (MC) algorithm and its variants: Markov chain MC (MCMC); Ensemble Kalman Filter (EnKF), or Sequential MC (SMC), to name by a few (*cf.* (Dashti & Stuart, 2016) and references therein). Typically, MC-based algorithms converge slowly, as $\mathcal{O}(M^{-1/2})$, for estimates of distribution moments, subject to M numerical solutions of the operator equation under consideration. Despite this slow convergence, MC algorithms are free from the *curse of dimensionality*, i.e. the convergence rate $\mathcal{O}(M^{-1/2})$ is ensured independently of the number of parameters in the model describing the uncertainty. An alternative to Monte Carlo methods are deterministic approaches that directly compute properties of the statistical distribution. Nevertheless, when the problem possesses *distributed random input data*, such as domain geometry, heterogeneous material properties, etc., these deterministic representations do suffer from the curse of dimensionality and the amount of work required to compute the representation of the solution increases exponentially in the number of dimensions. Example deterministic techniques are Karhúnen-Loève, Fourier or wavelet expansions of shapes and material properties. The deterministic representations lead to the mathematical problem of *high-dimensional interpolation and integration*, accompanied by numerical techniques such as polynomial chaos, Model Order Reduction (MOR) or the stochastic FEM (Beddek, Le Menach, Clenet, & Moreau, 2011; Du, Luo, & Kong, 2008).

In the present work, we apply the ideas developed by Schwab *et al.* (von Petersdorff & Schwab, 2006; Helmut Harbrecht & Schwab, 2008; Jerez-Hanckes & Schwab, 2017) to efficiently approximate statistical moments of the radiative transport solutions due to uncertainty in the sources. Broadly speaking, if the operators are deterministic, statistical moments can be taken directly on the unknowns and sources, thereby turning the problem into a tensorized deterministic one. The only requirement is knowledge of the sources' statistical moments. Though the problem considered is of higher dimension, the associated tensorized systems can be numerically solved without ever forming the tensor form matrix resulting from standard FEM. Moreover, by sparsifying the tensor systems, computational work and memory grows only poly-logarithmically in degrees of freedom. Application

of sparse tensor methods for transport equations without uncertainty was carried out by Schwab and co-workers (Schwab, Süli, & Todor, 2008; Schwab & Todor, 2006) reducing the number of degrees associated to angular and spatial directions. We will apply these techniques to several problems of multigroup neutron diffusion with prescribed source uncertainties. To reduce computational plexity, the combination technique developed by Harbrecht *et al.* (Harbrecht, Peters, & Siebenmorgen, 2013) is employed.

The article is structured as follows. Section 2 introduces our model problem with Sections 3 and 4 discussing variational formulations for the deterministic and stochastic versions, respectively. Of particular interest is the well-posedness of the problem and deterministic computation of statistical problems. Section 5 presents the numerical discretization scheme used along with convergence rates. As we will show both theoretically and numerically, standard FEM implementations lead to an error build-up arising from forward substitution for consecutive energy levels. As the number of energy groups grows, convergence worsens. We do not solve this issue here and it will constitute future work. Computational experiments are developed in Sections 6 and 7 for homogenous and non-homogenous random sources, respectively, validating our theoretical claims. Finally, conclusions and future research lines are sketeched in Section 9, with an appendix provided for completeness.

2. PRELIMINARIES

2.1. Notation

Throughout, scalar quantities will be denoted by normal fonts while vector ones by boldface. We write $\mathbb{N}$ for the set of natural numbers, $\mathbb{N}_0 := \mathbb{N} \cup \{0\}$, $\mathbb{R}$ the set of real numbers with $\mathbb{R}_+ := \{x \in \mathbb{R} : x > 0\}$.

Let $O \subset \mathbb{R}^d$, $d = 1, 2$, be an open and Lipschitz domain. For $k \in \mathbb{N}_0$, $\mathcal{C}^k(O)$ represents the space of k-times differentiable continuos functions. The class of p-integrable functions over O is $L^p(O)$ for $p \geq 1$. We denote the standard Sobolev spaces (Steinbach, 2007) by $H^s(O)$ for $s \in \mathbb{R}$, with $H^0(O) \equiv L^2(O)$, dual $\widetilde{H}^{-s}(O)$, and norms denoted by $\|\cdot\|_{H^s(O)}$. Duality pairings are denoted by $\langle \cdot, \cdot \rangle$ with subscripts indicating the domain of involved functional spaces, if it is not clear from the context. Similarly, inner products are written as $(\cdot, \cdot)$, only requiring integration domains as subscript.

2.2. Transport Equations and its parameters

The neutrons migration through a material medium can be modeled using the transport equation (Koeze, 2012):

$$\frac{1}{|v|}\frac{\partial}{\partial t}u(\mathbf{x}, \boldsymbol{\theta}, E, t) = -\boldsymbol{\theta} \cdot \nabla u(\mathbf{x}, \boldsymbol{\theta}, E, t) - \sigma_t(\mathbf{x}, E, t)u(\mathbf{x}, \boldsymbol{\theta}, E, t) + S_s(\mathbf{x}, \boldsymbol{\theta}, E, t) + S_f(\mathbf{x}, \boldsymbol{\theta}, E, t) + Q(\mathbf{x}, \boldsymbol{\theta}, E, t), \quad (2.1)$$

wherein $u(\mathbf{x}, \theta, E, t)$ is the neutron flux, the product of the phase space density of neutrons and the neutron speed, at $\mathbf{x} \in \mathcal{D} \subset \mathbb{R}^2$, travelling in direction $\theta \in \mathbb{R}^2$ at time $t \in \mathbb{R}$ and with an energy $E \in \mathbb{R}^+$. $\mathcal{D}$ can be an open bounded Lipschitz domain.

Since neutrons are neutral particles, they travel in straight lines between collisions with nuclei in the material medium. When this happens, the neutrons can be scattered in

another direction or absorbed. If it is absorbed in certain types of nuclei, nuclear fission can occur.

In equation (2.1) the σ parameters are known as macroscopic *cross sections* and have units of inverse length. The total cross section, σ_t, is the probability per unit distance travelled that a neutron has a collision with a nucleus, and the fractions $\frac{\sigma_s}{\sigma_t}$ and $\frac{\sigma_a}{\sigma_t}$ represent probabilities of scattering and absorption occurring per collision. When an absorption reaction occurs, the neutron can become a part of the nucleus or fission can occur: probabilities for either are given by $\frac{\sigma_\gamma}{\sigma_a}$ and $\frac{\sigma_f}{\sigma_a}$, respectively. When fission occurs, the energy of released neutrons has a distribution $\chi(E)$. $\nu(\mathbf{x}, E)$ is the average number of neutrons created per fission in the position $\mathbf{x}$ and energy level E.

As a balance equation, each term in (2.1) represents the following:

- Neutron advection $\boldsymbol{\theta} \cdot \nabla u(\mathbf{x}, \boldsymbol{\theta}, E, t)$
- Neutrons absorbed or scattered into another direction and energy level represent a loss in the angular flux and can be quantified as $\sigma_t(\mathbf{x}, t, E)u(\mathbf{x}, \boldsymbol{\theta}, E, t)$
- Neutron gain corresponding to neutrons scattering from direction and energy $(\hat{\boldsymbol{\theta}}, \hat{E})$ to $(\boldsymbol{\theta}, E)$. This contribution, $S_s(\mathbf{x}, \boldsymbol{\theta}, E, t)$, is

$$S_s(\mathbf{x}, \boldsymbol{\theta}, E, t) := \int_{\mathbb{S}} \int_0^\infty \sigma_S(\mathbf{x}, \hat{\boldsymbol{\theta}} \to \boldsymbol{\theta}, \hat{E} \to E, t) u(\mathbf{x}, \hat{\boldsymbol{\theta}}, \hat{E}, t) d\hat{E} d\hat{\boldsymbol{\theta}}$$

- The production of neutrons from fission $S_f(\mathbf{x}, \boldsymbol{\theta}, E, t)$ with

$$S_f(\mathbf{x}, \boldsymbol{\theta}, E, t) := \frac{\chi(E)}{4\pi} \int_{\mathbb{S}} \int_0^\infty \nu(\mathbf{x}, E) \sigma_f(\mathbf{x}, \hat{\boldsymbol{\theta}}, \hat{E}) u(\mathbf{x}, \hat{\boldsymbol{\theta}}, \hat{E}, t) d\hat{E} d\hat{\boldsymbol{\theta}}$$

- External sources that release neutrons, $Q(\mathbf{x}, \boldsymbol{\theta}, E, t)$.

2.3. Steady State and Multigroup Energy Approximation

Assuming steady state and time-independent parameters, (2.1) is simplified into

$$0 = -\boldsymbol{\theta} \cdot \nabla u(\mathbf{x}, \boldsymbol{\theta}, E) - \sigma_t(\mathbf{x}, E) u(\mathbf{x}, \boldsymbol{\theta}, E) + S_s(\mathbf{x}, \boldsymbol{\theta}, E) + S_f(\mathbf{x}, \boldsymbol{\theta}, E) + Q(\mathbf{x}, \boldsymbol{\theta}, E) \tag{2.2}$$

The multigroup energy approximation relies on discretizing E to build energy groups. Each energy group includes all the neutrons with energy in a certain range. Let the energy range $[\mathcal{E}_0, \mathcal{E}_{N_E}]$ with $\mathcal{E}_{N_E} > \mathcal{E}_0 \geq 0$ be partitioned into N_E non-overlapping intervals $[\mathcal{E}_{N_E - e}, \mathcal{E}_{Ne-e+1}]$; the interval $[\mathcal{E}_{N_E-e}, \mathcal{E}_{N_E-e+1}]$ is called *energy group* $e = 1, \ldots, N_E$.

$$u^{(e)}(\mathbf{x}, \theta) = \int_{\mathcal{E}_{e-1}}^{\mathcal{E}_e} u(\mathbf{x}, \boldsymbol{\theta}, E) dE$$

Using this approximation with $N_E \in \mathbb{N}$ energy groups, we can write equation (2.2) as (Stacey, 2007),

$$\begin{aligned} 0 = -\boldsymbol{\theta} \cdot \nabla u^{(e)}(\mathbf{x}, \boldsymbol{\theta}) - \sigma_t^{(e)}(\mathbf{x}) u^{(e)}(\mathbf{x}, \boldsymbol{\theta}) \\ + \sum_{\hat{e}=1}^{N_E} \int_{\mathbb{S}} \sigma_S^{(\hat{e} \to e)}(\mathbf{x}, \hat{\boldsymbol{\theta}} \to \boldsymbol{\theta}) u^{(\hat{e})}(\mathbf{x}, \hat{\boldsymbol{\theta}})) d\hat{\boldsymbol{\theta}} \\ + \sum_{\hat{e}=1}^{N_E} \frac{\chi^{(e)}}{4\pi} \int_{\mathbb{S}} \nu^{(e)}(\mathbf{x}) \sigma_f(\mathbf{x}, \hat{\boldsymbol{\theta}}) u^{(\hat{e})}(\mathbf{x}, \hat{\boldsymbol{\theta}}) d\hat{\boldsymbol{\theta}} + Q^{(e)}(\mathbf{x}, \boldsymbol{\theta}), \end{aligned} \tag{2.3}$$

where each parameter now depends on the energy group and are computed based on a weighted average with an assumed energy profile.

2.4. Diffusion Equation

If we further assume isotropic scattering and a bounded and piecewise continous source (Larsen & Morel, 1989; Evans, 2015), the transport equation asymptotically limits to a diffusion equation.

We will work in two-dimensional physical domain though the whole program can directly be extended to 3D. Let $\mathcal{D} \subset \mathbb{R}^2$ be an open bounded Lipschitz domain. The migration of neutrons through a material medium can be modeled using the multigroup neutron diffusion equation (Bell & Glasstone, 1970; Stacey, 2007):

$$-\nabla \cdot D^{(e)}(\mathbf{x})\nabla u^{(e)}(\mathbf{x}) + \sigma_r^{(e)}(\mathbf{x})u^{(e)}(\mathbf{x}) - \sum_{\hat{e}\neq e} \sigma_s^{(\hat{e}\to e)}(\mathbf{x})u^{(\hat{e})}(\mathbf{x}) = f^{(e)}(\mathbf{x}), \quad \forall e = 1, \ldots, N_E, \quad (2.4)$$

wherein $u^{(e)}(\mathbf{x})$ is the neutron flux integrated over an energy range $[\mathcal{E}_{e-1}, \mathcal{E}_e]$, and is interpreted as the number density of neutrons at $\mathbf{x}$ multiplied by an average neutron speed. The removal cross-section $\sigma_r^{(e)}$ for group e is given by

$$\sigma_r^{(e)} = \sigma_a^{(e)} + \sum_{\hat{e}\neq e} \sigma_s^{(e\to\hat{e})},$$

where $\sigma_a^{(e)}$ is the absorption cross-section for energy group e at the position $\mathbf{x} \in \mathcal{D}$ with units of inverse length, and $\sigma_s^{(\hat{e}\to e)}$, is the scattering cross-section from energy group $\hat{e}$ to e at position $\mathbf{x} \in \mathcal{D}$. $D^{(e)}$ is the piecewise-constant energy group diffusion coefficient with units of length. Finally, $f^{(e)}$ is the prescribed source (in units of number density per unit time) of neutrons into energy group e at position $\mathbf{x}$.

ASSUMPTION 2.1. *In the following, we will assume cross-sections $\sigma_a^{(e)}$, $\sigma_s^{(\hat{e}\to e)}$ and diffusion coefficients to lie in $L^\infty(\mathcal{D})$ and be non-negative measurable functions satisfying the following* subcriticality conditions *(Bourhrara, 2006):*

$$0 < \sigma_0 \leq \sigma_r^{(e)} \leq \sigma_\infty, \quad (2.5)$$

$$\sigma_a^{(e)} + \sum_{e=1}^{N_E} \sigma_s^{(e\to\hat{e})} - \sum_{\hat{e}=1}^{N_E} \sigma_s^{(\hat{e}\to e)} \geq \alpha > 0, \quad (2.6)$$

$$\sigma_a^{(e)} \geq \alpha > 0, \quad (2.7)$$

for $\hat{e}, e = 1, \ldots, N_E$. These conditions imply that physically there can be no neutron chain reactions that do not end in finite time.

2.5. Boundary and interface conditions

Let $\mathcal{D} \subset \mathbb{R}^2$ be any open Lipschitz domain. We denote the standard Dirichlet and Neumann traces by γ_D and γ_N, respectively, defined over functions f in $\mathcal{C}^\infty(\mathcal{D})$ as

$$(\gamma_D f)(\mathbf{x}) := \lim_{\tilde{\mathbf{x}} \in \mathcal{D} \to \mathbf{x} \in \partial\mathcal{D}} f(\tilde{\mathbf{x}}), \qquad (\gamma_N f)(\mathbf{x}) := \lim_{\tilde{\mathbf{x}} \in \mathcal{D} \to \mathbf{x} \in \partial\mathcal{D}} \hat{\mathbf{n}} \cdot \nabla f(\tilde{\mathbf{x}}),$$

where $\mathbf{n}$ is the outward normal to the boundary $\partial\mathcal{D}$ and with known extensions (Steinbach, 2007) $\gamma_D : H^1(\mathcal{D}) \to H^{\frac{1}{2}}(\partial\mathcal{D})$ and $\gamma_N : H^1(\mathcal{D}) \to H^{-\frac{1}{2}}(\partial\mathcal{D})$.

On the boundary $\partial\mathcal{D}$, we will employ the so-called *Marshak boundary conditions*, which are mixed or Robin boundary conditions approximating no neutrons entering the domain (Brunner, Mehlhorn, McClarren, & Kurecka, 2005), for each energy group $e = 1, \ldots, N_E$,

$$\gamma_N u^{(e)}(\mathbf{x}) + \frac{1}{2D^{(e)}(\mathbf{x})} \gamma_D u^{(e)}(\mathbf{x}) = 0, \ \ \forall\, \mathbf{x} \in \partial\mathcal{D}. \tag{2.8}$$

If $\mathcal{D}$ is made up of different disjoint $N_{dom} \in \mathbb{N}$ subdomains, e.g., $\overline{\mathcal{D}} = \bigcup_{i=1}^{N_{dom}} \overline{\mathcal{D}}_i$, with $\mathcal{D}_i \cap \mathcal{D}_j = \emptyset$, for $i \neq j$, one may be required to state interface conditions. Without loss of generality, let us assume that $\mathcal{D}$ is composed of two such disjoint subdomains such that $\overline{\partial\mathcal{D}}_1 \cap \overline{\partial\mathcal{D}}_2 \neq \emptyset$ and that $u^{(e)}$ is solution of (2.4). Then, for $u_i^{(e)} := u^{(e)}|_{\mathcal{D}_i}$, $i = 1, 2$, being restrictions of the neutron flux over each subdomain, transmission conditions are given by (Duerigen, 2013):

$$\gamma_D^1 u_1^{(e)} = \gamma_D^2 u_2^{(e)} \qquad \text{on } \partial\mathcal{D}_1 \cap \partial\mathcal{D}_2, \tag{2.9a}$$

$$D_1^{(e)} \gamma_N^1 u_1^{(e)} = D_2^{(e)} \gamma_N^2 u_2^{(e)} \quad \text{on } \partial\mathcal{D}_1 \cap \partial\mathcal{D}_2, \tag{2.9b}$$

where $D_i^{(e)}$ is the constant value of the diffusion coefficient $D^{(e)}(\mathbf{x})$ inside the subdomain $\mathcal{D}_i$, $i = 1, 2$, respectively, and γ_D^i, γ_N^i, denote corresponding trace operators.

3. CONTINUOUS DETERMINISTIC MODEL

In what follows, we formally state the deterministic model problem of steady state neutron flux to be studied. Our setting will be that of H^1-spaces as in (Bourhrara, 2006); we also recall conditions for uniqueness and existence of solutions.

3.1. Deterministic Strong Formulation

For each energy group, let us define two operators:

$$\mathcal{A}^{(e)}u^{(e)} := \left(-\nabla \cdot D^{(e)}\nabla + \sigma_r^{(e)}\right) u^{(e)}, \tag{3.1}$$

$$\mathcal{B}^{(e\hat{e})}u^{(\hat{e})} := -\sigma_s^{(\hat{e}\to e)}u^{(\hat{e})}, \tag{3.2}$$

with $e = 1, \ldots, N_E$. Though coefficients and cross-sections may vary inside $\mathcal{D}$, our hypotheses allow us to conclude that both $\mathcal{A}^{(e)} : H^1(\mathcal{D}) \to \widetilde{H}^{-1}(\mathcal{D})$ and $\mathcal{B}^{(e)} : H^1(\mathcal{D}) \to H^1(\mathcal{D})$ are linear and continuous. Then, the strong formulation for the multigroup diffusion equation problem reads

PROBLEM 3.1. *For all $e = 1, \ldots, N_E$, let $f^{(e)} \in \widetilde{H}^{-1}(\mathcal{D})$. We seek $u \in H^1(\mathcal{D})$ such that*

$$\mathcal{A}^{(e)}u^{(e)} - \sum_{\hat{e}\neq e} \mathcal{B}^{(e\hat{e})}u^{(\hat{e})} = f^{(e)} \quad \textit{in } \mathcal{D}, \tag{3.3}$$

$$\gamma_N u^{(e)} + \frac{1}{2D^{(e)}}\gamma_D u^{(e)} = 0, \quad \textit{on } \partial\mathcal{D}. \tag{3.4}$$

Furthermore, we can define operator matrices $\mathbb{A} : [H^1(\mathcal{D})]^{N_E} \to [\widetilde{H}^{-1}(\mathcal{D})]^{N_E}$ and $\mathbb{B} : [H^1(\mathcal{D})]^{N_E} \to [\widetilde{H}^1(\mathcal{D})]^{N_E}$, to contain the operators for all energy groups:

$$\mathbb{A} := \operatorname{diag}(\mathcal{A}^{(1)}, \ldots, \mathcal{A}^{(N_E)}), \quad \mathbb{B} := \begin{bmatrix} 0 & \mathcal{B}^{(12)} & \cdots & \mathcal{B}^{(1N_E)} \\ \mathcal{B}^{(21)} & 0 & \cdots & \vdots \\ \vdots & \vdots & \ddots & \vdots \\ \mathcal{B}^{(N_E1)} & \mathcal{B}^{(N_E2)} & \cdots & 0 \end{bmatrix}. \tag{3.5}$$

Defining $\mathbb{D} := (\mathbb{A}+\mathbb{B})$ and setting $\mathbf{f} = (f^{(1)}, \ldots, f^{(N_E)})$ in $[\widetilde{H}^{-1}(\mathcal{D})]^{N_E}$, (3.3) can be equivalently written as,

$$\mathbb{D}(\mathbf{x})\mathbf{u}(\mathbf{x}) = \mathbf{f}(\mathbf{x}), \quad \forall\, \mathbf{x} \in \mathcal{D}, \tag{3.6}$$

where $\mathbf{u} = (u^{(1)}, \ldots, u^{(N_E)})$ in $[H^1(\mathcal{D})]^{N_E}$.

3.2. Deterministic Variational Formulation

For $e = 1, \ldots, N_E$, the variational form of Problem 3.1 can be written as

$$a^{(e)}(u^{(e)}, v) - \sum_{\hat{e}\neq e} b^{(\hat{e}e)}(u^{(e)}, v) = \left\langle f^{(e)}, v \right\rangle_{\mathcal{D}} \quad \forall\, v \in H^1(\mathcal{D}), \tag{3.7}$$

wherein the bilinear forms $a^{(e)}(\cdot,\cdot)$ and $b^{(\hat{e}e)}(\cdot,\cdot)$ are induced by the aforementioned operators as follows

$$\begin{aligned} a^{(e)}(u^{(e)}, v) &:= \int_{\mathcal{D}} D^{(e)}(\mathbf{x})\nabla u^{(e)}(\mathbf{x}) \cdot \nabla v(\mathbf{x}) d\mathbf{x} + \frac{1}{2}\int_{\partial\mathcal{D}} \gamma_D u^{(e)}(\mathbf{x})\gamma_D v(\mathbf{x}) d\mathbf{x} \\ &\quad + \int_{\mathcal{D}} \sigma_r^{(e)}(\mathbf{x}) u(\mathbf{x}) v(\mathbf{x}) d\mathbf{x}, \\ b^{(\hat{e}e)}(u^{(e)}, v) &:= -\int_{\mathcal{D}} \sigma_s^{(\hat{e}\to e)}(\mathbf{x}) u^{(e)}(\mathbf{x}) v(\mathbf{x}) d\mathbf{x}, \end{aligned}$$

by using integration-by-parts and the boundary condition (2.8). Clearly, both forms are continuous and bounded. However, it is less obvious to see that problem (3.7) is well posed.

Lemma 3.1 (Theorem 4 in (Bourhrara, 2006))**.** *Assume that the $u^{(\hat{e})} \in H^1(\mathcal{D})$ are given for $\hat{e} \neq e$. For $f^{(e)} \in L^2(\mathcal{D})$ and under subcriticality conditions* (2.5)–(2.7)*, problem* (3.7) *has a unique solution $u^{(e)} \in H^1(\mathcal{D})$, for each $e = 1, \ldots, N_E$.*

The proof is based on the Fredholm alternative (Steinbach, 2007, Theorem 3.35) and on the injectivity of the bilinear form for the case of subcritical conditions. In particular,

the coercivity estimates arise by shifting the compact pertubation provided by the substraction of mass terms multiplied by $\sigma_r^{(e)}$ and $\sigma_s^{(\hat{e}\to e)}$ and the compact embedding $H^1 \hookrightarrow L^2$ (*cf.* (Bourhrara, 2006; Hanuš, 2011) and (Steinbach, 2007)).

Similarly, we can state the variational formulation for the entire multigroup diffusion system (3.6) with boundary conditions (3.4) by considering the bilinear form:

$$d(\mathbf{u},\mathbf{v}) := \langle \mathbb{D}\,\mathbf{u},\mathbf{v}\rangle_{\mathcal{D}} = \sum_{e=1}^{N_E} a^{(e)}(u^{(e)},v^{(e)}) - \sum_{e=1}^{N_E}\sum_{\hat{e}\neq e} b^{(\hat{e}e)}(u^{(e)},v^{(e)}). \tag{3.8}$$

The above is derived by understanding the duality pairing over the Cartesian product space $[H^1(\mathcal{D})]^{N_E}$ as the sum over all N_E individual $H^1(\mathcal{D})$-pairings and using integration-by-parts formula.

PROBLEM 3.2. *Let* $\mathbf{f} \in [\widetilde{H}^{-1}(\mathcal{D})]^{N_E}$. *Find* $\mathbf{u} \in [H^1(\mathcal{D})]^{N_E}$ *such that*

$$d(\mathbf{u},\mathbf{v}) = \langle \mathbf{f},\mathbf{v}\rangle_{\mathcal{D}} \quad \forall\, \mathbf{v} \in [H^1(\mathcal{D})]^{N_E}, \tag{3.9}$$

where the source term is just the sum of individual dual products $\left\langle f^{(e)}, v\right\rangle_{\mathcal{D}}$ *over* e.

Corollary 3.1 (Theorem 7 in (Bourhrara, 2006))**.** *Assume* $\mathbf{f} \in [\widetilde{H}^{-1}(\mathcal{D})]^{N_E}$. *Then, Problem 3.2 has a unique solution* $\mathbf{u} \in [H^1(\mathcal{D})]^{N_E}$. *Moreover, the operator* $\mathbb{D}$ *is bounded and invertible .*

ASSUMPTION 3.1. *In order to obtain convergence estimates, we will later assume that there exist bounded mappings* $\mathbb{D}^{-1}$ *from* $[\widetilde{H}^{-1+s}(\mathcal{D})]^{N_E}$ *to* $[H^{1+s}(\mathcal{D})]^{N_E}$, *for* $0 \le s \le s_0$, *with* s_0 *depending on the domain regularity and smoothness of parameters and sources. We will not elaborate on this and point out the relevant work by Stewart (Stewart, 1974, 1976).*

4. CONTINUOUS STOCHASTIC MODEL

In equation (2.4), both source and parameters are deterministic. However, in reality, sources are composed of materials that release neutrons, involving epistemic and aleatoric uncertainties, as measurements are not accurate and neutrons behave differently each time the experiment is made. Similarly, cross-sections' uncertainties also suffer of such types of randomness (Zwermann et al., 2014).

4.1. Abstract Theory

In order to quantify uncertainty effects, we introduce parts of the theory presented in (von Petersdorff & Schwab, 2006; Jerez-Hanckes & Schwab, 2017). Let $(\Omega, \mathcal{F}, \mathbb{P})$ be a probability space, where, as customary, Ω denotes the set of all elementary events, $\mathcal{F}$ denotes the associated σ-algebra and $\mathbb{P}$ a probability measure. We define a random field g with values in a separable Hilbert space X as a strongly measurable mapping $g : \Omega \to X$ which maps events $E \in \mathcal{F}$ to Borel sets in X.This induces a measure $\tilde{\mathbb{P}}$ on X.

For $k \in \mathbb{N}$, the random variable $g : \Omega \to X$ lies in the Bochner space $L^k(\Omega, \mathbb{P}; X)$ if $\omega \mapsto \|g(\omega)\|_X^k$ is measurable and integrable, satisfying

$$\|g\|^k_{L^k(\Omega,\mathbb{P};X)} := \int_\Omega \|g(\omega)\|_X^k \mathrm{d}\mathbb{P}(\omega) < \infty.$$

If $g \in L^1(\Omega, \mathbb{P}; X)$, the expectation

$$\mathbb{E}[g] \ := \ \int_\Omega g(\omega)\mathrm{d}\mathbb{P}(\omega) \ \in \ X \tag{4.1}$$

exists as a Bochner integral with

$$\|\mathbb{E}[g]\|_X \ \leq \ \|g\|_{L^1(\Omega,\mathbb{P};X)} \, . \tag{4.2}$$

Let B belong to $\mathcal{L}(X, Y)$, the space of linear continuous mappings from X to Y. For a random variable g in $L^k(\Omega, \mathbb{P}; X)$ one constructs another random variable $h(\omega) = \mathsf{B}g(\omega) \in L^k(\Omega, \mathbb{P}; Y)$ satisfying

$$\|\mathsf{B}g\|_{L^k(\Omega,\mathbb{P};Y)} \;\leq\; \|g\|_{L^k(\Omega,\mathbb{P};X)}. \tag{4.3}$$

Furthermore,

$$\mathsf{B}\int_\Omega g(\omega)\mathrm{d}\mathbb{P}(\omega) \;=\; \int_\Omega \mathsf{B}g(\omega)\mathrm{d}\mathbb{P}(\omega)\,. \tag{4.4}$$

For $k \in \mathbb{N}$, the k-fold tensor product space is defined as

$$X^{(k)} \;:=\; \underbrace{X \otimes \cdots \otimes X}_{k\text{-times}} \tag{4.5}$$

equipped with the natural norm $\|\cdot\|_{X^{(k)}}$, which is a cross-norm, i.e.

$$\|g_1 \otimes \cdots \otimes g_k\|_{X^{(k)}} \;=\; \|g_1\|_X \cdots \|g_k\|_X\,, \tag{4.6}$$

for all $g_1, \ldots, g_k$ in X. Taking $\mathsf{B} \in \mathcal{L}(X,Y)$, there is a unique linear, continuous tensor product operator:

$$\mathsf{B}^{(k)} \;:=\; \underbrace{\mathsf{B} \otimes \cdots \otimes \mathsf{B}}_{k\text{-times}} \;\in\; \mathcal{L}(X^{(k)}, Y^{(k)})\,. \tag{4.7}$$

For a random field $u \in L^k(\Omega,\mathbb{P};X)$, let the k-fold simple tensor product $u^{(k)}(\omega) := u(\omega) \otimes \cdots \otimes u(\omega)$. Then, $u^{(k)} \in L^1(\Omega,\mathbb{P};X^{(k)})$. For $u \in L^k(\Omega,\mathbb{P};X)$ with finite $k \in \mathbb{N}$, the kth moment of $u(\omega)$ is defined by

$$\mathcal{M}^k u \;=\; \mathbb{E}\big[\underbrace{u \otimes \cdots \otimes u}_{k\text{-times}}\big] \;=\; \int_{\omega\in\Omega} \underbrace{u(\omega) \otimes \cdots \otimes u(\omega)}_{k\text{-times}}\,\mathrm{d}\mathbb{P}(\omega)\,. \tag{4.8}$$

Nonetheless, in the present work we will just focus on first and second order moments, i.e. $k = 1, 2$. Observe that, for $k \in \mathbb{N}$, we denote by $X^k = X \times ... \times X$ the k-fold Cartesian product of X, with graph norm given by the sum of k components. This is different from the k-fold tensor product $X^{(k)}$ in (4.5).

The next result justifies deterministic computations of first and second order statistical moments.

PROPOSITION 4.1 (Theorem 6.1 in (Jerez-Hanckes & Schwab, 2017)). *Assume given* $\mathsf{A} \in \mathcal{L}(X,Z)$, $\mathsf{B} \in \mathcal{L}(Y,Z)$ *for three Hilbert spaces* X, Y, Z, *with* A *boundedly invertible.*

Then, for $f \in L^2(\Omega, \mathbb{P}; Y)$, the solution of the operator stochastic equation:

$$\mathsf{A}u(\omega) = \mathsf{B}f(\omega) \tag{4.9}$$

admits a unique solution $u \in L^2(\Omega, \mathbb{P}; X)$ whose first and second moments, $\mathbb{E}[u] \in X$ and $\mathcal{M}^2 u := \mathbb{E}[u \otimes u] \in X^{(2)}$, respectively, uniquely solve the associated deteministic equations:

$$\mathsf{A}\mathbb{E}[u] = \mathsf{B}\mathbb{E}[f] \quad \textit{in} \quad Z \,, \tag{4.10}$$

and

$$(\mathsf{A} \otimes \mathsf{A})u^{(2)} = (\mathsf{B} \otimes \mathsf{B})\mathcal{M}^2 f \quad \textit{in} \quad Z^{(2)} \,, \tag{4.11}$$

where $\mathcal{M}^2 f := \mathbb{E}[f \otimes f] \in Y^{(2)}$.

4.2. First statistical moment

We now consider stochastic sources $f^{(e)}(\mathbf{x}, \omega)$ with $\omega \in (\Omega, \mathcal{F}, \mathbb{P})$. As in Section 3, we state the strong and variational formulations for the first statistical moment problem. As shorthand, we identify for brevity $X^s \equiv [H^{1+s}(\mathcal{D})]^{N_E}$ and $Z^s \equiv [\widetilde{H}^{-1+s}(\mathcal{D})]^{N_E}$, with $X \equiv X^0$ and $Z \equiv Z^0$ hereafter.

4.3. Strong Formulation

Assuming sources to be stochastic while keeping physical parameters deterministic, we rewrite Problem 3.1 as follows. Let $f^{(e)} \in L^1(\Omega, \mathbb{P}, \widetilde{H}^{-1}(\mathcal{D}))$ for $e = 1, \ldots, N_E$. For each realization $\omega \in (\Omega, \mathcal{F}, \mathbb{P})$, we seek $u^{(e)} \in L^1(\Omega, \mathbb{P}, H^1(\mathcal{D}))$ such that

$$\mathcal{A}^{(e)} u^{(e)}(\omega) - \sum_{\hat{e} \neq e} \mathcal{B}^{(e\hat{e})} u^{(\hat{e})}(\omega) \;=\; f^{(e)}(\omega) \quad \text{in } \mathcal{D}, \tag{4.12}$$

$$\gamma_N u^{(e)}(\omega) + \frac{1}{2D^{(e)}} \gamma_D u^{(e)}(\omega) \;=\; 0 \quad \text{on } \partial\mathcal{D} \tag{4.13}$$

for $e = 1, \ldots, N_E$. Equivalently and as before, (4.12) can be summarized as

$$\mathbb{D}(\mathbf{x})\mathbf{u}(\mathbf{x}, \omega) = \mathbf{f}(\mathbf{x}, \omega) \quad \forall\, \mathbf{x} \in \mathcal{D}, \tag{4.14}$$

where $\mathbf{u}$ now lies in the Bochner space $L^1(\Omega, \mathbb{P}, X)$ and $\mathbf{f}$ in $L^1(\Omega, \mathbb{P}, Z)$ with $\mathbb{D}$ defined in (3.5). As explained in Section 4.1, taking expectation on both sides of (4.14) yields

$$\mathbb{E}[\mathbb{D}\,\mathbf{u}] = \mathbb{E}[\mathbf{f}] \text{ in } \mathcal{D}. \tag{4.15}$$

Similarly, for (4.13), it holds

$$\mathbb{E}[\gamma_N u^{(e)}] + \frac{1}{2D^{(e)}}\mathbb{E}[\gamma_D u^{(e)}] = 0 \quad \text{ on } \partial\mathcal{D}, \quad \forall\, e = 1, \ldots, N_E. \tag{4.16}$$

As the spaces $H^1(\mathcal{D})$, $H^r(\partial\mathcal{D})$, for $|r| \leq \frac{1}{2}$, are separable, and operators $\mathbb{D}$, γ_N and γ_D are linear and deterministic, property (4.4) holds. Consequently, the strong first moment problem can be stated as

$$\begin{aligned} \mathbb{D}\,\mathbb{E}[\mathbf{u}] &= \mathbb{E}[\mathbf{f}] \quad \text{in } Z, & (4.17)\\ \gamma_N\mathbb{E}[u^{(e)}] + \frac{1}{2D^{(e)}}\gamma_D\mathbb{E}[u^{(e)}] &= 0 \qquad \text{on } \partial\mathcal{D}, \quad \forall\, e = 1, \ldots, N_E. & (4.18) \end{aligned}$$

For shorthand, let us define

$$\bar{\mathbf{u}}(\mathbf{x}) := \mathbb{E}[\mathbf{u}](\mathbf{x}) \quad \text{and} \quad \bar{\mathbf{f}}(\mathbf{x}) := \mathbb{E}[\mathbf{f}](\mathbf{x}).$$

Then, equation (4.17) turns into

$$\mathbb{D}\,\bar{\mathbf{u}} = \bar{\mathbf{f}} \quad \text{in } Z, \tag{4.19}$$

which, along with boundary conditions (4.18) become the strong deterministic formulation for the first moment problem.

4.4. Variational Formulation

By Corollary 3.1 and recalling the definition of the bilinear form $d(\cdot, \cdot)$ in (3.8), one can quickly derive the next result:

PROPOSITION 4.2. *Let* $\mathbf{f} \in L^1(\Omega, \mathbb{P}, Z)$ *with mean* $\bar{\mathbf{f}} \in Z$. *Then, the first order moment variational problem: seek* $\bar{\mathbf{u}} \in X$ *such that*

$$d(\bar{\mathbf{u}}, \mathbf{v}) = \sum_{e=1}^{N_E} \left\langle \bar{f}^{(e)}, v^{(e)} \right\rangle_{\mathcal{D}}, \tag{4.20}$$

for all $\mathbf{v} \in X$, *with* $\mathbf{v} = (v^{(1)}, \ldots, v^{(N_E)})$, *has a unique solution continuously dependent on the data.*

4.5. Second Statistical Moment Problem

We are interested on computing not only the first order but also the second order moment as well , so as to have more statistical information related to the neutron flux. Observe that this implies knowledge of the source's statistical second order moments $\mathcal{M}^2\mathbf{f}$. The following derivation is reminiscent to the one performed by Harbrecht (Harbrecht, 2014).

4.6. Strong Formulation

We assume that $\mathbf{f} \in L^2(\Omega, \mathbb{P}, Z)$ and seek $\mathbf{u} \in L^2(\Omega, \mathbb{P}, X)$. Taking second moments of (4.14) yields

$$\mathcal{M}^2[\mathbb{D}\,\mathbf{u}] \;=\; \mathcal{M}^2\mathbf{f} \text{ in } Z^{(2)} \tag{4.21}$$

as $\mathbb{D} \in \mathcal{L}(X, Z)$ and where $Z^{(2)} = Z \otimes Z$. When tensorizing, particular attention should be given to the Cartesian product space structures embedded in the definitions of spaces X, Z, i.e.

$$X^{(2)} = X \otimes X = [H^1(\mathcal{D})]^{N_E} \otimes [H^1(\mathcal{D})]^{N_E} = [H^1(\mathcal{D}) \otimes H^1(\mathcal{D})]^{N_E \times N_E}.$$

Let us define the bivariate spaces $H^r_{mix}(\mathcal{D} \times \mathcal{D}) := H^r(\mathcal{D}) \otimes H^r(\mathcal{D})$ and similarly for dual spaces. Then, we can identify

$$(X^s)^{(2)} = [H^{1+s}_{mix}(\mathcal{D} \times \mathcal{D})]^{N_E \times N_E} \text{ and } (Z^s)^{(2)} = [\widetilde{H}^{-1+s}_{mix}(\mathcal{D} \times \mathcal{D})]^{N_E \times N_E}.$$

Hence, we can use Proposition 4.1 to write

$$(\mathbb{D}\otimes\mathbb{D})\mathcal{M}^2\mathbf{u} = \mathcal{M}^2\mathbf{f} \text{ in } Z^{(2)}. \tag{4.22}$$

To further simplify notation, we define

$$U(\mathbf{x},\mathbf{y}) := (\mathcal{M}^2\mathbf{u})(\mathbf{x},\mathbf{y}) = \mathbb{E}[\mathbf{u}\otimes\mathbf{u}](\mathbf{x},\mathbf{y}) \in X^{(2)} \tag{4.23}$$

$$F(\mathbf{x},\mathbf{y}) := (\mathcal{M}^2\mathbf{f})(\mathbf{x},\mathbf{y}) = \mathbb{E}[\mathbf{f}\otimes\mathbf{f}](\mathbf{x},\mathbf{y}) \in Z^{(2)}. \tag{4.24}$$

For each energy level $e = 1,\dots,N_E$, we derive for the boundary conditions the following tensor deterministic equation on $\partial\mathcal{D}\times\partial\mathcal{D}$:

$$\mathcal{M}^2\left(\gamma_N u^{(e)}\right) = -\mathcal{M}^2\left(\frac{1}{2D^{(e)}}\gamma_D u^{(e)}\right) \tag{4.25}$$

$$(\gamma_N\otimes\gamma_N)\,\mathcal{M}^2 u^{(e)} = \left(\frac{1}{2D^{(e)}}\gamma_D\otimes\frac{1}{2D^{(e)}}\gamma_D\right)\mathcal{M}^2 u^{(e)} \tag{4.26}$$

This holds across energy groups $e\neq\hat{e}$. Moreover, these equations are meaningful at least in $H^{-\frac{1}{2}}_{mix}(\partial\mathcal{D}\times\partial\mathcal{D})$, and with more regularity as an equation in $L^2_{mix}(\partial\mathcal{D}\times\partial\mathcal{D})$.

With the above derivations, we can state the strong form of the second moment problem:

PROBLEM 4.1. *For $F\in Z^{(2)}$, seek $U\in X^{(2)}$ such that*

$$(\mathbb{D}\otimes\mathbb{D})U = F \qquad \text{in } \mathcal{D}\times\mathcal{D}, \tag{4.27}$$

$$(\mathbb{D}\otimes\gamma_D)U = 0 \qquad \text{in } \mathcal{D}\times\partial\mathcal{D}, \tag{4.28}$$

$$(\gamma_D\otimes\mathbb{D})U = 0 \qquad \text{in } \partial\mathcal{D}\times\mathcal{D}, \tag{4.29}$$

$$(\gamma_N\otimes\gamma_N)\,U^{(e\hat{e})} = \left(\frac{1}{2D^{(e)}}\gamma_D\otimes\frac{1}{2D^{(\hat{e})}}\gamma_D\right)U^{(e\hat{e})} \qquad \text{on } \partial\mathcal{D}\times\partial\mathcal{D}, \tag{4.30}$$

for energy levels $1\leq e,\hat{e}\leq N_E$.

Observe that (4.28) and (4.29) complete the system. Finally, Dirichlet and Neumann trace operators in Problem 4.1 should be interpreted as Cartesian arrays of trace operators per energy group.

4.7. Variational Formulation

The variational formulation of Problem 4.1 is built by taking duality products of (4.27) over $X^{(2)}$. In what follows, we precise the variable dependence and recall that $X^{(2)} = [H^1_{mix}(\mathcal{D}\times\mathcal{D})]^{N_E\times N_E}$. By integration-by-parts and using equations (4.25), (4.28) and (4.29), we arrive at the following problem

PROBLEM 4.2. *Seek $U \in X^{(2)}$ such that, for any $F \in Z^{(2)}$, it holds*

$$d_2(U,V) = \langle F, V\rangle_{\mathcal{D}}\,, \quad \forall\, V \in X^{(2)}, \tag{4.31}$$

wherein now there is a sum of $N_E \times N_E$ duality pairings in $H^1_{mix}(\mathcal{D}\times\mathcal{D})$ and the bilinear form $d_2(\cdot,\cdot)$ is defined as:

$$\begin{aligned} d_2(U,V) := &\sum_{e_1,e_2=1}^{N_E} a_2^{(e_1e_2)}(U^{(e_1e_2)},V) + \sum_{e_1,\hat{e}_1,e_2,\hat{e}_2=1}^{N_E} b_2^{(\hat{e}_1\hat{e}_2e_1e_2)}(U^{(\hat{e}_1\hat{e}_2)},V) \\ &+ \sum_{e_1,e_2,\hat{e}_2=1}^{N_E} ab^{(e_1\hat{e}_2e_2)}(U^{(e_1\hat{e}_2)},V) + \sum_{\hat{e}_1,e_1,e_2=1}^{N_E} ba^{(e_1\hat{e}_1e_2)}(U^{(\hat{e}_1e_2)},V) \end{aligned} \tag{4.32}$$

for all $V \in H^1_{mix}(\mathcal{D}\times\mathcal{D})$, with the following terms:

$$\begin{aligned} a_2^{(e_1e_2)}(U^{(e_1e_2)},V) := &\int_{\mathcal{D}\times\mathcal{D}} (D^{(e_1)}(\mathbf{x})\nabla_{\mathbf{x}} \otimes D^{(e_2)}(\mathbf{y})\nabla_{\mathbf{y}})U^{(e_1e_2)}(\mathbf{x},\mathbf{y})(\nabla_{\mathbf{x}}\otimes\nabla_{\mathbf{y}})V(\mathbf{x},\mathbf{y})d\mathbf{x}d\mathbf{y} \\ &+ \frac{1}{2}\int_{\mathcal{D}\times\partial\mathcal{D}} (D^{(e_1)}(\mathbf{x})\nabla_{\mathbf{x}} \otimes \gamma_D)U^{(e_1e_2)}(\mathbf{x},\mathbf{y})(\nabla_{\mathbf{x}}\otimes\gamma_D)V(\mathbf{x},\mathbf{y})d\mathbf{x}ds_{\mathbf{y}} \\ &+ \frac{1}{2}\int_{\partial\mathcal{D}\times\mathcal{D}} (\gamma_D \otimes D^{(e_2)}(\mathbf{y})\nabla_{\mathbf{y}})U^{(e_1e_2)}(\mathbf{x},\mathbf{y})(\gamma_D\otimes\nabla_{\mathbf{y}})V(\mathbf{x},\mathbf{y})ds_{\mathbf{x}}d\mathbf{y} \\ &+ \frac{1}{4}\int_{\partial\mathcal{D}\times\partial\mathcal{D}} (\gamma_D \otimes \gamma_D)U^{(e_1e_2)}(\mathbf{x},\mathbf{y})(\gamma_D\otimes\gamma_D)V(\mathbf{x},\mathbf{y})ds_{\mathbf{x}}ds_{\mathbf{y}} \end{aligned}$$

$$
\begin{aligned}
&+ \int\limits_{\mathcal{D}\times\mathcal{D}} (D^{(e_1)}(\mathbf{x})\nabla_{\mathbf{x}} \otimes \sigma_r^{(e_2)}(\mathbf{y}))U^{(e_1e_2)}(\mathbf{x},\mathbf{y})(\nabla_{\mathbf{x}} \otimes \mathcal{I}_{\mathbf{y}})V(\mathbf{x},\mathbf{y})d\mathbf{x}d\mathbf{y} \\
&+ \int\limits_{\mathcal{D}\times\mathcal{D}} (\sigma_r^{(e_1)}(\mathbf{x}) \otimes D^{(e_1)}(\mathbf{y})\nabla_{\mathbf{y}})U^{(e_1e_2)}(\mathbf{x},\mathbf{y})(\mathcal{I}_x \otimes\nabla_{\mathbf{y}})V(\mathbf{x},\mathbf{y})d\mathbf{x}d\mathbf{y} \\
&+ \frac{1}{2}\int\limits_{\mathcal{D}\times\partial\mathcal{D}} (\sigma_r^{(e_1)}(\mathbf{x}) \otimes \gamma_D)U^{(e_1e_2)}(\mathbf{x},\mathbf{y})(\mathcal{I}_{\mathbf{x}} \otimes\gamma_D)V(\mathbf{x},\mathbf{y})d\mathbf{x}ds_{\mathbf{y}} \\
&+ \frac{1}{2}\int\limits_{\partial\mathcal{D}\times\mathcal{D}} (\gamma_D \otimes \sigma_r^{(e_2)}(\mathbf{y}))U^{(e_1e_2)}(\mathbf{x},\mathbf{y})(\gamma_D \otimes \mathcal{I}_{\mathbf{y}})V(\mathbf{x},\mathbf{y})ds_{\mathbf{x}}d\mathbf{y} \\
&+ \int\limits_{\mathcal{D}\times\mathcal{D}} (\sigma_r^{(e_1)}(\mathbf{x}) \otimes \sigma_r^{(e_2)}(\mathbf{y}))U^{(e_1e_2)}(\mathbf{x},\mathbf{y})V(\mathbf{x},\mathbf{y})d\mathbf{x}d\mathbf{y},
\end{aligned}
$$

$$
b_2^{(\hat{e}_1\hat{e}_2e_1e_2)}(U^{(\hat{e}_1\hat{e}_2)},V) \;:=\; -\int\limits_{\mathcal{D}\times\mathcal{D}} (\sigma_s^{(\hat{e}_1\to e_1)}(\mathbf{x}) \otimes \sigma_s^{(\hat{e}_2\to e_2)}(\mathbf{y}))U^{(\hat{e}_1\hat{e}_2)}(\mathbf{x},\mathbf{y})V(\mathbf{x},\mathbf{y})d\mathbf{x}d\mathbf{y},
$$

$$
\begin{aligned}
ab^{(e_1\hat{e}_2e_2)}(U^{(e_1\hat{e}_2)},V) \;:=\; &\int\limits_{\mathcal{D}\times\mathcal{D}} (D^{(e_1)}(\mathbf{x})\nabla_{\mathbf{x}} \otimes \sigma_s^{(\hat{e}_2\to e_2)}(\mathbf{y}))U^{(e_1\hat{e}_2)}(\mathbf{x},\mathbf{y})(\nabla_{\mathbf{x}} \otimes \mathcal{I}_{\mathbf{y}})V(\mathbf{x},\mathbf{y})d\mathbf{x}d\mathbf{y} \\
&-\frac{1}{2}\int\limits_{\partial\mathcal{D}\times\mathcal{D}} (\gamma_D \otimes \sigma_s^{(\hat{e}_2\to e_2)}(\mathbf{y}))U^{(e_1\hat{e}_2)}(\mathbf{x},\mathbf{y})V(\mathbf{x},\mathbf{y})d\mathbf{x}d\mathbf{y} \\
&-\int\limits_{\mathcal{D}\times\mathcal{D}} (\sigma_a^{(e_1)}(\mathbf{x}) \otimes \sigma_s^{(\hat{e}_2\to e_2)}(\mathbf{y}))U^{(e_1\hat{e}_2)}(\mathbf{x},\mathbf{y})V(\mathbf{x},\mathbf{y})d\mathbf{x}d\mathbf{y}.
\end{aligned}
$$

The bilinear form $ba(\cdot,\cdot)$ follows the same pattern as $ab(\cdot,\cdot)$ and we do not include it here for the sake of brevity.

By Corollary 3.1, $\mathbb{D}$ is boundedly invertible and consequently direct use of Proposition 4.1 leads to the well-posedness of the tensor deterministic Problem 4.2 for the second order moment.

PROPOSITION 4.3. *Let* $\mathbf{f} \in L^2(\Omega, \mathbb{P}, Z)$ *with second order moment* $F \in Z^{(2)}$. *Then, the second order moment variational Problem 4.2 has a unique solution* $U \in X^{(2)}$ *continuously dependent on the data.*

5. NUMERICAL DISCRETIZATION

We now present the details of the FEM implementation for the multigroup diffusion problem performed as well as associated convergence rates. As stated initially, the main advantage of the deterministic approach for statistical moments relies on the availability of a standard FEM code to solve the tensorized second order moment. As we will show, this process never requires actual tensorization and can be efficiently computed with poly-logarithmic effort in terms of degrees of freedom.

5.1. Discretization of the deterministic problem

We seek to approximate the variational formulation for the nuclear flux diffusion problem described in Problem 3.2. We consider a sequence of nested meshes $\{\mathcal{T}_{N_h}\}_{N_h\in\mathbb{N}}$, each one composed of triangular elements $\{\tau_t\}_{t=1}^{N_h}$, characterized by a meshwidth $h > 0$ and such that

$$\overline{\mathcal{D}} = \overline{\mathcal{T}}_{N_h} = \bigcup_{t=1}^{N_h} \overline{\tau}_t.$$

We will later on refer to mesh discretization levels $l \in \mathbb{N}_0$, for which the meshwidth $h(l)$ yields $N_{h(l)}$ degrees of freedom and one may write N_l for brevity.

Discrete solutions $\mathbf{u}_h(\mathbf{x})$ will belong to the finite element space $[V_h]^{N_E}$, where V_h is defined as

$$V_h := \{v_h \in H^1(\mathcal{D}) : v_h|_{\tau_i} \in \mathbb{P}_1(\tau_i) \quad \forall\, i = 1, \ldots, N_h\}. \tag{5.1}$$

Let $\varphi_i^h(\mathbf{x})$ denote the basis functions of V_h, i.e. $V_h = \operatorname{span}\{\varphi_1^h, ..., \varphi_{N_h}^h\}$. Then, the Cartesian product approximation space can be written as

$$[V_h]^{N_E} = \operatorname{span}\{\boldsymbol{\varphi}_i^{h,e}\}_{i,e=1}^{N_h,N_E}$$

where $\boldsymbol{\varphi}_i^{h,e}$ is defined as

$$\boldsymbol{\varphi}_i^{h,e}(\mathbf{x}) := \varphi_i^h(\mathbf{x})\hat{c}_e$$

and $\hat{c}_e \in \mathbb{R}^{N_E}$ is the canonic vector non-zero at group e. Consequently, the unknown

$$\mathbf{u}_h(\mathbf{x}) = \sum_{e=1}^{N_E} \sum_{i=1}^{N_h} \mathrm{u}_i^{(e)} \boldsymbol{\varphi}_i^{h,e}(\mathbf{x}) \tag{5.2}$$

where $\mathrm{u}_i^{(e)} \in \mathbb{R}$ are unknown coefficients. Using equation (3.9) and test functions given by the same basis functions $\boldsymbol{\varphi}_i^{h,e}$, we write down the Galerkin discrete problem:

PROBLEM 5.1. *Let* $\mathbf{f} \in Z$. *Find* $\mathbf{u}_h \in [V_h]^{N_E}$ *such that*

$$d(\mathbf{u}_h, \mathbf{v}_h) = \langle \mathbf{f}, \mathbf{v}_h \rangle_{\mathcal{D}} \quad \forall\, \mathbf{v}_h \in [V_h]^{N_E}, \tag{5.3}$$

with $d(\cdot,\cdot)$ *as defined in* (3.8)*.*

By conformity and denseness of the V_h in X and injectivity of $\mathbb{D}$ (*cf.* Corollary 3.1), one can prove the following result:

Lemma 5.1 (Thm. 8.11 in (Steinbach, 2007))**.** *There exists a refinement level* $h_0 > 0$ *such that the following stability condition*

$$c_s \|\mathbf{w}_h\|_X \leq \sup_{0 \neq \mathbf{v}_h \in [V_h]^{N_E}} \frac{d(\mathbf{w}_h, \mathbf{v}_h)}{\|\mathbf{v}_h\|_X} \quad \forall\, \mathbf{w}_h \in X, \tag{5.4}$$

holds for all $0 \leq h < h_0$*, with a bounded constant* $c_s > 0$*.*

Armed with the above stability condition, we derive the next proposition as in (Steinbach, 2007, Thm. 8.10).

PROPOSITION 5.1. *Problem 5.1 has a unique solution* $\mathbf{u}_h \in [V_h]^{N_E}$*. Moreover, the best approximation error bound holds*

$$\|\mathbf{u} - \mathbf{u}_h\|_X \leq \left(\frac{c_{\mathbb{D}}}{c_s}\right) \inf_{\mathbf{v}_h \in V_h} \|\mathbf{u} - \mathbf{v}_h\|_X, \tag{5.5}$$

where $c_{\mathbb{D}}$ *is the continuity constant of* $\mathbb{D}$*.*

5.1.1. Matrix formulation

By replacing the discrete solution in the energy group e

$$u_h^{(e)}(\mathbf{x}) = \sum_{i=1}^{N_h} \mathrm{u}_i^{(e)} \varphi_i^h(\mathbf{x}) \tag{5.6}$$

in the definitions for $a^{(e)}$ and $b^{(\hat{e}e)}$ in Section 3.2, we derive Galerkin matrices: $A^{(e)} := \left(a_{ij}^{(e)}\right)_{i,j=1}^{N_h}$, $B^{(e\hat{e})} := \left(b_{ij}^{(e\hat{e})}\right)_{i,j=1}^{N_h}$ and $\mathbf{f}^{(e)} := \left(f_i^{(e)}\right)_{i=1}^{N_h}$, with

$$a_{ij}^{(e)} := a^{(e)}(\varphi_j^h, \varphi_i^h), \quad b_{ij}^{(e\hat{e})} := b^{(e\hat{e})}(\varphi_j^h, \varphi_i^h), \quad f_i^{(e)} := \left\langle f^{(e)}, \varphi_i^h \right\rangle_{\mathcal{D}}, \tag{5.7}$$

for $e = 1, \ldots, N_E$. Thus, equation (5.3) can be equivalently written as a linear system as follows,

$$\begin{bmatrix} A^{(1)} & B^{(12)} & \cdots & B^{(1N_E)} \\ B^{(21)} & A^{(2)} & \cdots & B^{(2N_E)} \\ \vdots & \vdots & \ddots & \vdots \\ B^{(N_E1)} & B^{(N_E2)} & \cdots & A^{(N_E)} \end{bmatrix} \begin{bmatrix} \mathbf{u}^{(1)} \\ \mathbf{u}^{(2)} \\ \vdots \\ \mathbf{u}^{(N_E)} \end{bmatrix} = \begin{bmatrix} \mathbf{f}^{(1)} \\ \mathbf{f}^{(2)} \\ \vdots \\ \mathbf{f}^{(N_E)} \end{bmatrix} \tag{5.8}$$

5.1.2. Convergence Error

We now provide theoretical convergence rates for Galerkin Problem 5.1 using piecewise-linear approximation basis. For this, we recall the following standard result:

Lemma 5.2 (Thm. 9.10 in (Steinbach, 2007))**.** *Let O be a bounded Lipschitz domain and $u \in H^s(O)$ with $s \in [\beta, 2]$ and $\beta = 0,\ 1$. Then, there holds the approximation property:*

$$\inf_{v_h \in V_h(O)} \|u - v_h\|_{H^\beta(O)} \leq c h^{s-\beta} |u|_{H^s(O)}, \tag{5.9}$$

where $|\cdot|_{H^s(O)}$ denotes the $H^s(O)$-semi-norm and $V_h(O)$ the space of piecewise linear functions over a mesh on O.

We can derive a general error bound in the Cartesian product space framework by assuming Assumption 3.1 and combining the above lemma with Proposition 5.1.

PROPOSITION 5.2. *Let $\beta = 0, 1$ and $\mathbf{u} \in X^\beta$ and $\mathbf{u}_h \in V_h$ denote the continuous and discrete solutions of Problem 3.2 and 5.1, respectively. Then, the following error bound holds*

$$\|\mathbf{u} - \mathbf{u}_h\|_{X^\beta} \leq ch^{s-\beta} \sum_{e=1}^{N_E} \left|u^{(e)}\right|_{H^s(\mathcal{D})}, \tag{5.10}$$

for $s \in [\beta, 2]$ and with a constant $c > 0$.

Alternatively, using Cea's Lemma (Steinbach, 2007, Thm. 8.1) and Lemma 5.2 we can derive the following error bound for the first energy group:

PROPOSITION 5.3. *Assume there is only down-scattering and $u^{(1)} \in H^\beta(\mathcal{D})$, with $\beta = 0, 1$. Then, it holds*

$$\|u^{(1)} - u_h^{(1)}\|_{H^\beta(\mathcal{D})} \leq \frac{c_2^{A^{(1)}}}{c_1^{A^{(1)}}} \inf_{v_h^{(1)} \in V_h} \|u^{(1)} - v_h^{(1)}\|_{H^\beta(\mathcal{D})} \leq Ch^{s-\beta} \left|u^{(1)}\right|_{H^s(\mathcal{D})} \tag{5.11}$$

with $s \in [\beta, 2]$ and $C := \frac{c_2^{\mathcal{A}^{(1)}}}{c_1^{\mathcal{A}^{(1)}}} c$ and constants $c_2^{\mathcal{A}^{(1)}}$ and $c_1^{\mathcal{A}^{(1)}}$ being continuity and coercivity constants of the operator $\mathcal{A}^{(1)}$.

In general, the same inequality for all the energy groups does not hold due to the lack of Galerkin orthogonality. Consequently, the interaction between the energy groups generates a dependence between the errors of different groups. Theorem 5.1 states the relation between every group with the first one in a down-scattering diffusion multigroup equation.

Theorem 5.1. *Let us consider the discrete solution given by solving the system* (5.8)*, when $\sigma_s^{(e_1 e_2)} = 0$ for all $e_1 > e_2$ (downscattering problem). The bound of the error of the multigroup diffusion equation approximate solution for an specific energy group e is*

bounded by an expression that includes the term

$$\prod_{e'=1}^{e-1} \frac{2}{c_1^{\mathcal{A}^{(e'+1)}}} \|\sigma_s^{(e'\to e'+1)}\|_{L^\infty} \|u^{(1)} - u_h^{(1)}\|_{L^2} \tag{5.12}$$

i.e.,

$$\|u^{(e)} - u_h^{(e)}\|_{L^2} \leq C^{(e)} + \prod_{e'=1}^{e-1} \frac{2}{c_1^{\mathcal{A}^{(e'+1)}}} \|\sigma_s^{(e'\to e'+1)}\|_{\infty} \|u^{(1)} - u_h^{(1)}\|_{L^2} \tag{5.13}$$

PROOF. See Appedix A □

This implies that the error of the first level is propagated to all the other levels. The same happens with each level lower than e. As we can see, the higher the σ_s values are and the lower the ellipticity constant is, the worst the error bound obtained.

5.2. Approximations of first and second moments

For the first moment problem described in Section 4.4, we simply require solving Problem 5.1 with a right-hand side equal to the expectation of the source $\bar{\mathbf{f}}$ using the standard FEM. The Galerkin matrices obtained will be reused for the second moment computation as follows.

For the second statistical moment (*cf.* Problem 4.2), we recall that each element $U^{(e_1e_2)} \in H^1_{mix}(\mathcal{D}\times\mathcal{D})$, with $e_1, e_2 \in \{1,\ldots,N_E\}$, can be approximated as a tensor product

$$U^{(e_1e_2)}(\mathbf{x},\mathbf{y}) = u^{(e_1)}(\mathbf{x})u^{(e_2)}(\mathbf{y}),$$

with $u^{(e_1)}$ and $u^{(e_2)}$ in $H^1(\mathcal{D})$. These in turn can be computed via $u_h^{(e_1)} \in V_h$ and $u_{\tilde{h}}^{(e_2)} \in V_{\tilde{h}}$, conforming finite element spaces in $H^1(\mathcal{D})$ as defined in (5.1) with h and $\tilde{h}$ not necessarily equal, i.e. their corresponding number of degrees of freedom N_h and $N_{\tilde{h}}$ may differ. In other words, we will seek

$$U_{h,\tilde{h}}^{(e_1e_2)} \in V_{h,\tilde{h}} := V_h \otimes V_{\tilde{h}},$$

where $N_{h,\tilde{h}} := \dim(V_{h,\tilde{h}}) = N_h \cdot N_{\tilde{h}}$.

We can now state the discrete version of Problem 4.2.

PROBLEM 5.2. *Seek* $U_h \in [V_{h,\tilde{h}}]^{N_E \times N_E}$ *such that, for any* $F \in Z^{(2)}$*, it holds*

$$d_2(U_{h\tilde{h}}, W_{h\tilde{h}}) = \langle F, W_{h\tilde{h}} \rangle_{\mathcal{D}}\,, \quad \forall\, W_h \in [V_{h,\tilde{h}}]^{N_E \times N_E}, \tag{5.14}$$

where the bilinear form $d_2(\cdot,\cdot)$ *is defined as in* (4.32)*.*

5.2.1. Matrix formulation

Again, let $\{\varphi_i^h\}_{i=1}^{N_h}$ and $\{\varphi_i^{\tilde{h}}\}_{i=1}^{N_{\tilde{h}}}$ denote basis functions for V_h and $V_{\tilde{h}}$, respectively. Then, one can define Cartesian product spaces

$$[V_h]^{N_E} \;=\; \operatorname{span}\{\boldsymbol{\varphi}_i^{h,e}\}_{i,e=1}^{N_h,N_E}, \quad [V_{\tilde{h}}]^{N_E} = \operatorname{span}\{\boldsymbol{\varphi}_i^{\tilde{h},e}\}_{i,e=1}^{N_{\tilde{h}},N_E} \tag{5.15}$$

where $\boldsymbol{\varphi}_i^{h,e}$ and $\boldsymbol{\varphi}_i^{\tilde{h},e}$ are defined as in Section 5.1. Then,

$$\mathbf{u}_h(\mathbf{x}) \;=\; \sum_{e_1=1}^{N_E}\sum_{i=1}^{N_h} \mathrm{d}_i^{(e_1)} \boldsymbol{\varphi}_i^{h,e_1}(\mathbf{x}) = \sum_{i=1}^{N_h} \mathbf{d}_i \varphi_i^h(\mathbf{x}) \tag{5.16}$$

$$\mathbf{u}_{\tilde{h}}(\mathbf{y}) \;=\; \sum_{e_2=1}^{N_E}\sum_{j=1}^{N_{\tilde{h}}} \tilde{\mathrm{d}}_j^{(e_2)} \boldsymbol{\varphi}_j^{\tilde{h},e_2}(\mathbf{y}) = \sum_{j=1}^{N_{\tilde{h}}} \tilde{\mathbf{d}}_j \varphi_j^{\tilde{h}}(\mathbf{y}) \tag{5.17}$$

With these, we can write

$$\begin{aligned} U_{h,\tilde{h}}(\mathbf{x},\mathbf{y}) &= \left(\sum_{e_1=1}^{N_E}\sum_{i=1}^{N_h} \mathrm{d}_i^{(e_1)} \boldsymbol{\varphi}_i^{h,e_1}(\mathbf{x})\right)\left(\sum_{e_2=1}^{N_E}\sum_{j=1}^{N_{\tilde{h}}} \tilde{\mathrm{d}}_j^{(e_2)} \boldsymbol{\varphi}_j^{\tilde{h},e_2}(\mathbf{y})\right)^T \\ &= \sum_{i=1}^{N_h}\sum_{j=1}^{N_{\tilde{h}}} \mathbf{d}_i \tilde{\mathbf{d}}_j^T \varphi_i^h(\mathbf{x}) \varphi_j^{\tilde{h}}(\mathbf{y}) \end{aligned} \tag{5.18}$$

where $\mathbf{d}_i, \tilde{\mathbf{d}}_j \in \mathbb{R}^{N_E}$ are the unknown coefficient vectors for $i = 1,\ldots,N_h$ and $j = 1,\ldots,N_{\tilde{h}}$, respectively. Replacing (5.18) in (5.14) and using as test functions the tensor basis

$$\left\{\boldsymbol{\varphi}_i^{h,e_1}(\mathbf{x})\boldsymbol{\varphi}_j^{\tilde{h},e_2}(\mathbf{y})^T\right\}_{i,j,e_1,e_2=1}^{N_h,N_{\tilde{h}},N_E,N_E},$$

we obtain the following linear system:

$$\left(\sum_{k=1}^{N_h} A_{ik}\mathbf{d}_k\right)\left(\sum_{l=1}^{N_{\tilde{h}}} \widetilde{A}_{jl}\tilde{\mathbf{d}}_l\right)^T = \mathbf{Q}_{ij} \quad \forall\, i=1,\ldots,N_h,\ \forall\, j=1,\ldots,N_{\tilde{h}}, \tag{5.19}$$

where matrices $A_{ik} \in \mathbb{R}^{N_E\times N_E}$, for all $i,k = 1,\ldots,N_h$ and $\widetilde{A}_{jl} \in \mathbb{R}^{N_E\times N_E}$ for all $j,l = 1,\ldots,N_{\tilde{h}}$, are defined as,

$$A_{ik} := \begin{bmatrix} a_{ik}^{(1)} & b_{ik}^{(12)} & \ldots & b_{ik}^{(1N_E)} \\ b_{ik}^{(21)} & a_{ik}^{(2)} & \ldots & b_{ik}^{(2N_E)} \\ \vdots & \vdots & \ddots & \vdots \\ b_{ik}^{(N_E1)} & b_{ik}^{(N_E2)} & \ldots & a_{ik}^{(N_EN_E)} \end{bmatrix}, \quad \widetilde{A}_{jl} := \begin{bmatrix} \widetilde{a}_{jl}^{(1)} & \widetilde{b}_{jl}^{(12)} & \ldots & \widetilde{b}_{jl}^{(1N_E)} \\ \widetilde{b}_{jl}^{(21)} & \widetilde{a}_{jl}^{(2)} & \ldots & \widetilde{b}_{jl}^{(2N_E)} \\ \vdots & \vdots & \ddots & \vdots \\ \widetilde{b}_{jl}^{(N_E1)} & \widetilde{b}_{jl}^{(N_E2)} & \ldots & \widetilde{a}_{jl}^{(N_EN_E)}, \end{bmatrix}$$

where entries $a_{ik}^{(e_1)}$, $b_{ik}^{(e_1\hat{e_1})}$ and are defined over V_h as in (5.7) for $e_1,\hat{e_1} = 1,\ldots,N_E$. Similarly for $\widetilde{a}_{jl}^{(e_2)}$ and $\widetilde{b}_{jl}^{(e_2\hat{e_2})}$ over $V_{\tilde{h}}$. The source second moment terms $\mathbf{Q}_{ij} \in \mathbb{R}^{N_E\times N_E}$ are defined as,

$$\mathbf{Q}_{ij} := \int\limits_{\mathcal{D}\times\mathcal{D}} F(\mathbf{x},\mathbf{y})\varphi_i^h(\mathbf{x})\varphi_j^{\tilde{h}}(\mathbf{y})d\mathbf{x}d\mathbf{y}, \tag{5.20}$$

for $i = 1,\ldots,N_h$ and $j = 1,\ldots,N_{\tilde{h}}$. Equivalently, one can write (5.19) as

$$\sum_{k=1}^{N_h}\sum_{l=1}^{N_{\tilde{h}}} A_{ik}\mathbf{D}_{kl}\widetilde{A}_{jl}^T \;=\; \mathbf{Q}_{ij}, \tag{5.21}$$

where $\mathbf{D}_{kl} := \mathbf{d}_k\tilde{\mathbf{d}}_l^T \in \mathbb{R}^{N_E\times N_E}$. This is the same as the following matrix system

$$\begin{bmatrix} A_{11}\begin{bmatrix} \widetilde{A}_{11}^T & \ldots & \widetilde{A}_{1N_{\hat{h}}}^T \\ \vdots & \ddots & \vdots \\ \widetilde{A}_{N_{\hat{h}}1}^T & \ldots & \widetilde{A}_{N_{\hat{h}}N_{\hat{h}}}^T \end{bmatrix} & \ldots & A_{1N_h}\begin{bmatrix} \widetilde{A}_{11}^T & \ldots & \widetilde{A}_{1N_{\hat{h}}}^T \\ \vdots & \ddots & \vdots \\ \widetilde{A}_{N_{\hat{h}}} & \ldots & \widetilde{A}_{N_{\hat{h}}N_{\hat{h}}}^T \end{bmatrix} \\ \vdots & \ddots & \\ A_{N_h1}\begin{bmatrix} \widetilde{A}_{11}^T & \ldots & \widetilde{A}_{1N_{\hat{h}}}^T \\ \vdots & \ddots & \vdots \\ \widetilde{A}_{N_{\hat{h}}1}^T & \ldots & \widetilde{A}_{N_{\hat{h}}N_{\hat{h}}}^T \end{bmatrix} & \ldots & A_{N_hN_h}^T\begin{bmatrix} \widetilde{A}_{11}^T & \ldots & \widetilde{A}_{1N_{\hat{h}}}^T \\ \vdots & \ddots & \vdots \\ \widetilde{A}_{N_h1}^T & \ldots & \widetilde{A}_{N_{\hat{h}}N_{\hat{h}}}^T \end{bmatrix} \end{bmatrix} \begin{bmatrix} \mathbf{D}_{11} \\ \vdots \\ \mathbf{D}_{1N_{\hat{h}}} \\ \vdots \\ \mathbf{D}_{N_h1} \\ \vdots \\ \mathbf{D}_{N_hN_{\hat{h}}} \end{bmatrix} = \begin{bmatrix} \mathbf{Q}_{11} \\ \vdots \\ \mathbf{Q}_{1N_{\hat{h}}} \\ \vdots \\ \mathbf{Q}_{N_h1} \\ \vdots \\ \mathbf{Q}_{N_hN_{\hat{h}}} \end{bmatrix} \tag{5.22}$$

Clearly, the above linear system has enormously increased the number of unknowns as the curse of dimensionality would predict.

PROPOSITION 5.4. *Define*

$$\mathbf{A} := \begin{bmatrix} A_{11} & \dots & A_{1N_h} \\ \vdots & \ddots & \vdots \\ A_{N_h 1} & \cdots & A_{N_h N_h} \end{bmatrix}, \qquad \widetilde{\mathbf{A}} := \begin{bmatrix} \widetilde{A}_{11} & \dots & \widetilde{A}_{1N_{\hat{h}}} \\ \vdots & \ddots & \vdots \\ \widetilde{A}_{N_{\hat{h}} 1} & \cdots & \widetilde{A}_{N_{\hat{h}} A_{\hat{h}}} \end{bmatrix}. \tag{5.23}$$

Then, equation (5.22) *can be equivalently written as*

$$\mathbf{A}\mathbf{D}\widetilde{\mathbf{A}}^T = \mathbf{Q}, \tag{5.24}$$

where $\mathbf{D} := (\mathbf{D}_{ij})_{i,j=1}^{N_h, N_{\hat{h}}}$ *and* $\mathbf{Q} := (\mathbf{Q}_{ij})_{i,j=1}^{N_h, N_{\hat{h}}}$.

PROOF. Let us define $\mathbf{Y} := \mathbf{D}\widetilde{\mathbf{A}}^T$, then

$$Y_{kj} \;=\; \sum_{l=1}^{N_{\hat{h}}} \mathbf{D}_{kl} \left(\widetilde{\mathbf{A}}^T\right)_{lj} = \sum_{l=1}^{N_{\hat{h}}} \mathbf{D}_{kl} \widetilde{\mathbf{A}}^T_{jl}$$

On the other hand, $\mathbf{Q} = \mathbf{A}\mathbf{Y}$, and therefore

$$\mathbf{Q}_{ij} \;=\; \sum_{k=1}^{N_{h_0}} A_{ik} Y_{kj} = \sum_{k=1}^{N_h} A_{ik} \sum_{l=1}^{N_{\hat{h}}} \mathbf{D}_{kl} \widetilde{A}^T_{jl} = \sum_{k=1}^{N_h} \sum_{l=1}^{N_{\hat{h}}} A_{ik} \mathbf{D}_{kl} \widetilde{A}^T_{jl}$$

as stated. □

Proposition 5.4 is important because it avoids dealing with the huge matrix system given by (5.22). Instead, we solve equation (5.24) in two steps,

$$\mathbf{A}\mathbf{Y} = \mathbf{Q} \quad \text{and} \quad \widetilde{\mathbf{A}}\mathbf{D}^T = \mathbf{Y}^T \tag{5.25}$$

One may wonder whether one could exploit for computational purposes choices h and $\hat{h}$. Indeed, as we will see one can compute the second moment using $\hat{h} = h$ and carry out a *full tensor discretization*. However, an *sparse* approximation will be shown to exist with considerable gains.

5.2.2. Full Tensor Approximation

We now switch notation from h to l, to explicitly declare the dependence of solutions on mesh refinement levels $L \in \mathbb{N}_0$ and associated spaces V_L. Thus, we will seek solutions $U_L(\mathbf{x}, \mathbf{y})$ in the tensor space

$$V_{L,L}^{N_E} := [V_L \otimes V_L]^{N_E \times N_E},$$

where we denote $V_L \equiv V_{h(L)}$. We can now state the following stability result:

Lemma 5.3. *There exists $L_0 \in \mathbb{N}$ and $c_S > 0$ such that for all $L \geq L_0$,*

$$\inf_{0 \neq U \in V_{L,L}^{N_E}} \sup_{0 \neq W \in V_{L,L}^{N_E}} \frac{d_2(U, W)}{\|U\|_{X^{(2)}} \|W\|_{X^{(2)}}} \geq \frac{1}{c_S} > 0. \tag{5.26}$$

PROOF. Follows directly from Lemma 5.1. □

With this tensor inf-sup condition, one can easily show that the full tensor product approximation for Problem 5.2 is unique.

PROPOSITION 5.5. *Problem 5.2 has a unique discrete solution $U_{L,L} \in V_{L,L}^{N_E}$. Moreover, if $U \in X^{(2)}$ denotes the solution of the continuous Problem 4.2, then*

$$\|U - U_{L,L}\|_{X^{(2)}} \leq c \inf_{W_{L,L} \in V_{L,L}^{N_E}} \|U - W_h\|_{X^{(2)}}, \tag{5.27}$$

with $c > 0$ bounded.

In this case, the basis elements φ_i^h and $\varphi_i^{\tilde{h}}$ will be equal and consequently also matrices $\mathbf{A}$ and $\widetilde{\mathbf{A}}$. Consequently, we just need to solve (5.25) computing only one matrix. However, the number of degrees of freedom using this full tensor technique is $N_{L,L} N_E^2 = (N_L \cdot N_E)^2$. Unfortunately, if one seeks to compute the solution for high discretization levels, the number of degrees of freedom will increase very fast and require large computational efforts.

5.2.3. Sparse Tensor Approximation

To tackle the curse of dimensionality, we introduce the sparse tensor approach following (von Petersdorff & Schwab, 2006) and later references (Harbrecht, Schneider, & Schwab, 2008; Hiptmair, Jerez-Hanckes, & Schwab, 2013). In a nutshell, the idea is to reduce the number of degrees of freedom by solving over a subspace of $V_{L,L}$.

For a nested sequence of meshes and associated finite element spaces $\{V_l\}_{l=0}^{L}$, one can define detail spaces W_l as

$$W_l := (P_l - P_{l-1})H^1(\mathcal{D}) \subset V_l, \quad l \geq 1,$$

where P_l is the projection into V_l space. Hence, one can write $V_L = W_L \oplus V_{L-1}$ and deduce

$$V_L = \bigoplus_{l=0}^{L} W_l,$$

where $W_0 := V_0$. The sparse tensor approximation consists of looking for the solution in the tensor space

$$\widehat{V}_{L,L_0} = \bigoplus_{\substack{2L_0 \leq i+j \leq L+L_0 \\ L_0 \leq i,j \leq L}} (W_i \otimes W_j) \tag{5.28}$$

where $L_0 \geq 0$ shall be referred to as *minimal resolution level*. This value is related to the threshold mesh required for asymptotic convergence and is characteristic of indefinite or coercive problems (Hiptmair et al., 2013; Jerez-Hanckes & Schwab, 2017).

Similar to the full tensor case, let us define

$$\widehat{V}_{L,L_0}^{N_E} := [\widehat{V}_{L,L_0}]^{N_E \times N_E}.$$

Then, we can state the next stability condition.

Lemma 5.4 (Thm. 5.2 in (von Petersdorff & Schwab, 2006))**.** *There exists* $L_0 \in \mathbb{N}$ *and* $\hat{c}_S > 0$ *such that for all* $L \geq L_0$*,*

$$\inf_{0\neq\widehat{U}\in\widehat{V}^{N_E}_{L,L_0}} \sup_{0\neq\widehat{W}\in\widehat{V}^{N_E}_{L,L_0}} \frac{d_2(\widehat{U},\widehat{W})}{\|\widehat{U}\|_{X^{(2)}}\|\widehat{W}\|_{X^{(2)}}} \geq \frac{1}{\hat{c}_S} > 0. \tag{5.29}$$

Moreover, the discrete problem is well posed.

PROPOSITION 5.6. *Let* $L_0 \in \mathbb{N}$ *and* $U \in X^{(2)}$ *the solution of Problem 4.2. Then, for any* $L \geq L_0$ *the sparse tensor version of Problem 5.1 has a unique solution* $\widehat{U}_{L,L_0} \in \widehat{V}^{N_E}_{L,L_0}$*. Moreover, it holds*

$$\|U - \widehat{U}_{L,L_0}\|_{X^{(2)}} \leq c \inf_{\widehat{W}_{L,L_0}\in\widehat{V}^{N_E}_{L,L_0}} \|U - \widehat{W}_{L,L_0}\|_{X^{(2)}}, \tag{5.30}$$

with $c > 0$ *bounded.*

5.2.4. Convergence Errors

Convergence rates for the full tensor approximation are obtained in a similar way to those for the first moment problem and we recall Assumption 3.1.

Denote the continuous solution $U^{(e_1e_2)} \in H^1_{mix}(\mathcal{D}\times\mathcal{D})$ and $U^{(e_1e_2)}_{L,L} \in V_{L,L}$ its full tensor Galerkin approximation. Then, by Proposition 5.5, it holds

$$\|U^{(e_1e_2)} - U^{(e_1e_2)}_{L,L}\|_{L^2(\mathcal{D}\times\mathcal{D})} \leq C \inf_{W_{L,L}\in V_{L,L}} \|U^{(e_1e_2)} - W_{L,L}\|_{L^2(\mathcal{D}\times\mathcal{D})}. \tag{5.31}$$

Then, by Lemma 5.2 with $O = \mathcal{D}\times\mathcal{D}$, we have the following result,

$$\|U^{(e_1e_2)} - U^{(e_1e_2)}_{L,L}\|_{H^\sigma(\mathcal{D}\times\mathcal{D})} \leq Ch^{s-\sigma} \left|U^{(e_1e_2)}\right|_{H^s(\mathcal{D}\times\mathcal{D})} \tag{5.32}$$

More generally, we can write

PROPOSITION 5.7. *Let* $\beta = 0, 1$. *Denote by* $U \in (X^\beta)^{(2)}$ *and* $U_{L,L} \in V_{L,L}^{N_E}$ *the solutions of Problems 4.2 and 5.2, respectively. Then, it holds*

$$\|U - U_{L,L}\|_{(X^\beta)^{(2)}} \leq c h^{s-\beta} \sum_{e_1,e_2=1}^{N_E} \left|U^{(e_1 e_2)}\right|_{H^s(\mathcal{D}\times\mathcal{D})} \tag{5.33}$$

for $s \in [\beta, 2]$ *and with a constant* $c > 0$.

Observe that the convergence in terms of h is the same for full tensor and first moment. However, in terms of degrees of freedom it differs, because $h \sim \mathcal{O}(N_L^{-2})$ and $h \sim \mathcal{O}(N_{L,L}^{-4})$ for first moment and full tensor approximations, respectively.

To state the theoretical result for the sparse tensor approximation we use (von Petersdorff & Schwab, 2006, Thm 5.3)

Lemma 5.5. *Assume* $\mathbf{f} \in L^2(\Omega, \mathbb{P}, Z^s)$ *with expectation* $\bar{\mathbf{f}}$*, and the approximation property given by* (5.9)*. Moreover, let* $U \in X^{(2)}$ *and* $\widehat{U}_{L,L_0} \in V_{L,L_0}^{N_E}$ *denote the solution for the continuous and discrete second moment Problems 4.2 and 5.2, respectively, and where* s *is the regularity of the continuous solution. Then, for* $0 \leq s \leq \min\{s_0, 1\}$*, it holds*

$$\|U - \widehat{U}_{L,L_0}\|_{X^{(2)}} \leq C N_L^{-s/2} \log(N_L)^{1/2} \|\bar{\mathbf{f}}\|_{Z^s}. \tag{5.34}$$

5.3. Combination technique

When working with meshes in more than one dimension it is hard to find explicitly basis functions for detail spaces W_l. Hence, we use the so-called *combination technique* (Harbrecht et al., 2013) to express (5.28) as sums of spaces $V_{l_1} \otimes V_{l_2}$. Specifically, one can write

$$\widehat{V}_{L,L_0} = \bigoplus_{l_1=L_0}^{L} V_{L+L_0-l_1} \otimes V_{l_1} \;\ominus\; \bigoplus_{l_2=L_0}^{L} V_{l_2} \otimes V_{L+L_0-l_2} \tag{5.35}$$

Thus, when looking for the solution $\widehat{U}_{L,L_0} \in \widehat{V}_{L,L_0}^{N_E}$, one needs to solve different linear systems over the tensor product spaces that are in equation (5.35). For sparse Tensor, the

number of degrees of freedom is the sum over all the combination of the spaces $(V_{l_1} \otimes V_{l_2})$ such that (l_1,l_2). For full tensor approximations, the number of degrees of freedom corresponds to the space $(V_L \otimes V_L)$ where L is the discretization level.

6. NUMERICAL RESULTS AND DISCUSSION FOR AN HOMOGENEOUS DOMAIN

6.1. Domain and parameters of the problem

The domain $\mathcal{D} \in \mathcal{R}^2$ chosen for this problem is defined as $\mathcal{D} := \{(x, y) \in \mathbb{R}^2 : 0 \leq x \leq 12, 0 \leq y \leq 12\}$. This domain is made up of water, whose parameters for removal cross section and diffusion coefficient are shown in Table C.1 (Appendix C) and domain $\mathcal{D}_b$. The parameters for the scattering cross section are shown in Tables B.1 and B.2 (Appendix B)

Meshes were constructed using the software GMSH [1], with refinement done by splitting. As a result of this procedure, we obtained 7 nested meshes defining 7 different discretization levels (L), with subspaces denoted by V_L, $L = \{1...7\}$. Again, we denote by N_L the number of degrees of freedom for each discretization level. To compute the FEM matrices we used FEniCS in Python.

6.2. Analytic Solution

First, we built the problem for a known analytic solution using the method of manufactured solutions (Lingus, 1971; Knupp & Salari, 2002; McClarren & Lowrie, 2008), in order to analyze the error between this and the discrete approximate solution.

We will use a solution with the general form given by equation (6.1)

$$u^{(e)}(x) = \frac{1}{D^{(e)}}(1 + \alpha^{(e)}x + \beta^{(e)}x^2)(1 + \alpha^{(e)}y + \beta^{(e)}y^2) \tag{6.1}$$

where $\alpha^{(e)}$ and $\beta^{(e)}$ should be such that $u^{(e)}$ meets the boundary conditions given by equation (2.8). It holds that,

[1] Available in `http://gmsh.info/`

$$\alpha^{(e)} = \frac{1}{2D^{(e)}} \qquad \beta^{(e)} = -\frac{(2 + 12\alpha^{(e)})}{(48D^{(e)} + 12^2)}$$

6.3. First Moment Convergence

In Figure 7.3 we show the error between the discrete and analytic solution for the first moment, at six different discretization levels. Each curve represents the error convergence of an specific energy group.

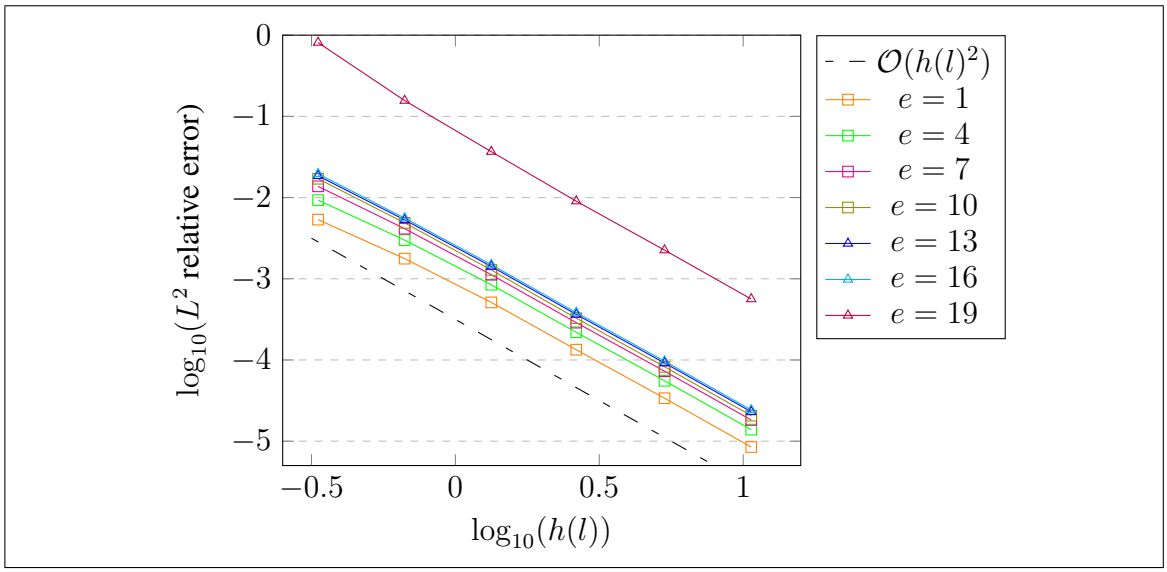

Figure 6.1. L^2-relative error between the discrete solution $\tilde{u}_l^{(e)}(\mathbf{x})$ and the analytic solution $\tilde{u}^{(e)}(\mathbf{x})$, for $l = \{1, 2, ..., 6\}$. h is the largest edge of the mesh used to define each discrete function space. The convergence is $\mathcal{O}(h(l)^2)$, as we expect from Proposition 5.1 and Theorem Lemma 5.2. The curves of the other energy groups have the same slope but are shifted up as predicted by Theorem 5.1.

As we can see in Figure 7.3, the error of each energy group is converging as we refine the mesh. We can also see, that the error is lower for the first energy group and increases with each subsequent group. This demonstrates the results in Section 5.1.2: the error bound of the higher groups is a nondecreasing function of the error in the lower energy groups when there is downscattering.

6.4. Second Moment Convergence

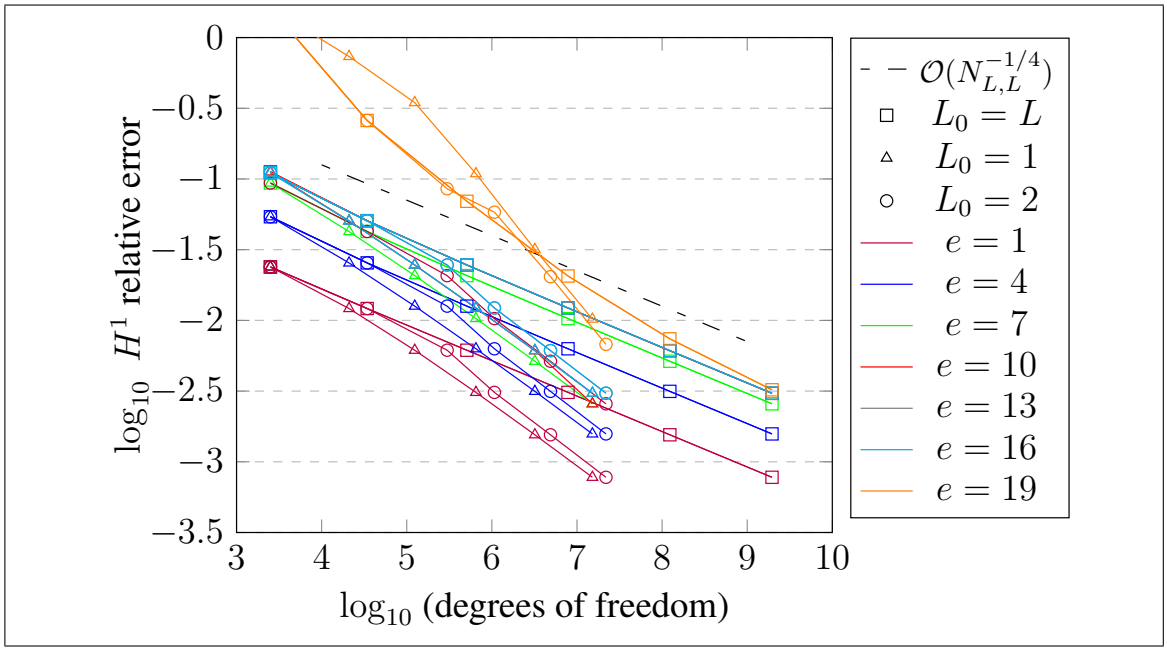

Figure 6.2. H^1 relative error between the discrete solution $U^{(ee)}_{L,L_0}(\mathbf{x},\mathbf{x})$ and the analytic solution $U^{(ee)}(\mathbf{x},\mathbf{x})$ for $e = \{1,2,3,4\}$, $l = \{1,2,...,6\}$. The discrete solution was obtained using Sparse Tensor and Full Tensor. In the case of Full Tensor, the convergence is $\mathcal{O}(N_{L,L}^{-1/4})$ where $N_{L,L} = N_L^2$ is the total number of degrees of freedom. This convergence is equivalent to $\mathcal{O}(h(L))$ where $h(L)$ is the mesh size.

For the second moment of the solution we compare the errors from the sparse and full tensors methods in Figure 6.2. In this figure both the sparse and full tensor solutions are

converging to the analytic solution. However, to achieve an specific error, the sparse tensor requires fewer degrees of freedom.

This is the result we expected for the sparse tensor method. Choosing an specific subset of the basis of the whole tensorized space, we can achieve similar errors using many fewer degrees of freedom.

Furthermore, we can also see in Figure 6.2 that the rate of convergence of the Full Tensor approximation is $\mathcal{O}(N_{L,L}^{-1/4})$, which is equivalent to $\mathcal{O}(N_L^{-1/2})$ and $\mathcal{O}(h)$. To demonstrate the theoretical convergence rate predicted in Figure 5.5 we plot the error in the sparse tensor results in terms of N_L in Figure 6.3. This figure demonstrates that the sparse tensor error agrees with the theoretical prediction for a second moment with regularity 1.

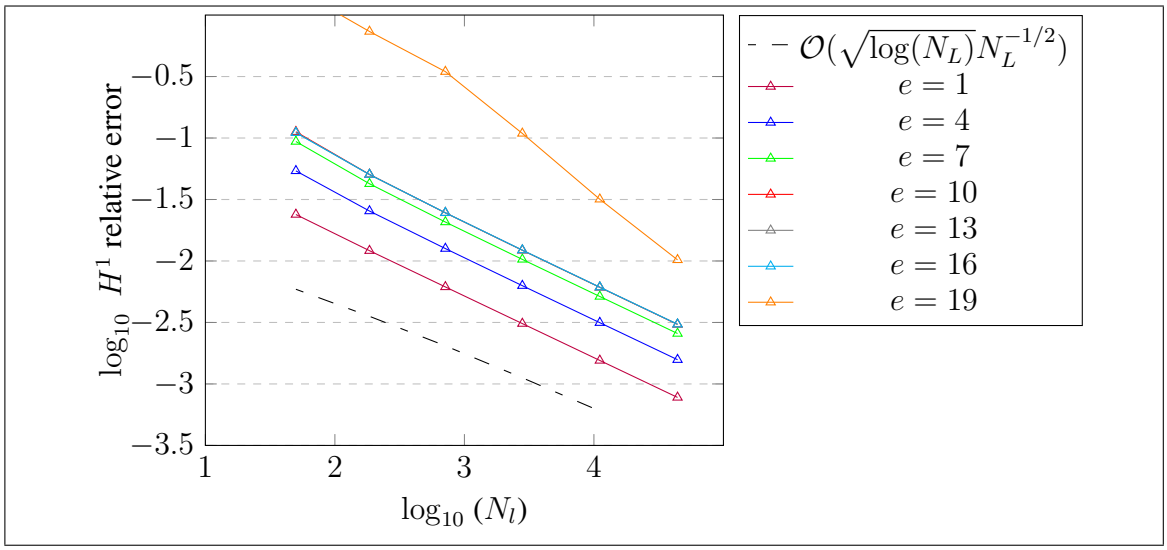

Figure 6.3. H^1 relative error between the discrete solution $U_{L,L_0}^{(ee)}(\mathbf{x},\mathbf{x})$, and the analytic solution $U^{(ee)}(\mathbf{x},\mathbf{x})$ for $L = \{1, 2, ..., 6\}$ and $L_0 = 1$. The convergence is $\mathcal{O}(\sqrt{\log(N_L)}N_L^{-1/2})$.

7. NUMERICAL RESULTS AND DISCUSSION FOR A NON-HOMOGENEOUS DOMAIN

We now turn to the more practically interesting non-homogeneous problems. In these problems the material properties will be functions of space.

We consider a generic radiation shielding problem where a neutron source (a plutonium spontaneous fission source) is immersed in water along with a heavy metal absorber (lead). The problem layout is illustrated in Figure 7.1.

7.1. Domain and parameters of the problem

To describe the domain we are going to define three different regions or subdomains: a bulk media ($\mathcal{D}_b$), a source region ($\mathcal{D}_s$) and an absorption region ($\mathcal{D}_a$).

$$\begin{aligned} \mathcal{D}_s &= \{(x,y) \in \mathbb{R}^2 : 2 \leq x \leq 4, 2 \leq y \leq 4\} \\ \mathcal{D}_a &= \{(x,y) \in \mathbb{R}^2 : 0 \leq x \leq 12, 0 \leq y \leq 12\} \\ \mathcal{D}_b &= \mathcal{D} - (\mathcal{D}_s \cup \mathcal{D}_a) \end{aligned}$$

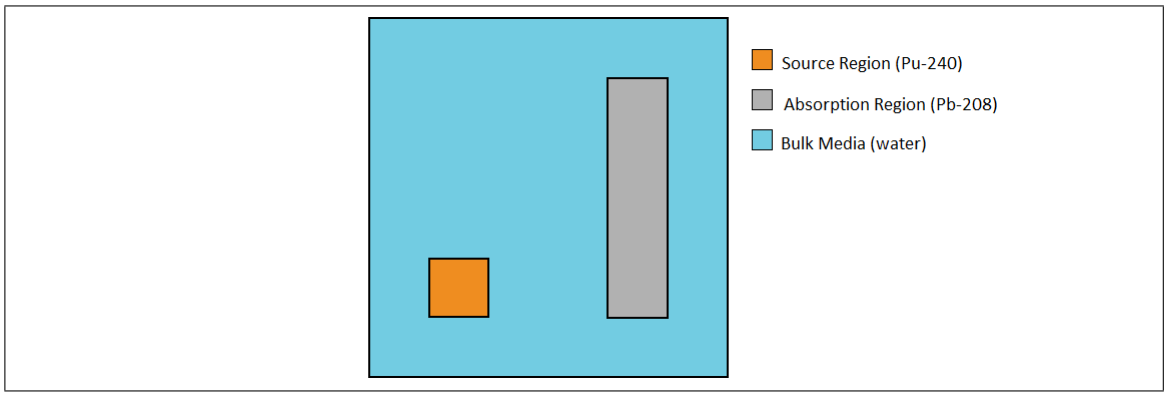

Figure 7.1. Layout of non-homogeneous problem containing a source, absorber, and a water background media.

In the case of a non-homogeneous domain, $\sigma_a^{(e)}(\mathbf{x})$, $\sigma_s^{(e_1 \to e_2)}(\mathbf{x})$, $D^{(e)}(\mathbf{x})$ are the absorption cross section, scatter cross section and difussion coefficient respectively, for energy group e at the position $\mathbf{x}$. This coefficients are constant in each subdomain. The absorption and diffusion parameters are shown in Table C.1.

7.2. Functions for the first and second moment of the source

The function chosen for the first moment of the source is

$$f^{(e)}(\mathbf{x}) = \begin{cases} \mu^{(e)} & \text{if } \mathbf{x} \in \mathcal{D}_s \\ 0 & \text{otherwise} \end{cases} \tag{7.1}$$

The values of μ are found in Table C.1.

The function chosen for the second moment of the source depends on the distance between the two points and the two energy groups, it is given by

$$u^{(e_1 e_2)}(x, y) = \begin{cases} C_1 \mu^{(e_1)} \mu^{(e_2)} \exp(-||x - y||_2 - C_2 |\bar{e}_1 - \bar{e}_2|) + \mu^{(e_1)} \mu^{(e_2)} & \text{if } x \in \mathcal{D}_s \\ 0 & \text{otherwise} \end{cases} \tag{7.2}$$

where $\bar{e}$ is the medium value of the energy level range of group e, $C_1 = 0.4$ and $C_2 = 100$.

7.3. First Moment Convergence

As we do not know the analytic solution, to compute the error we compare the discrete solution of each discretization level with the higher one computed.

In this case, we compute discrete solutions for 7 different discretization levels. In Figure 7.2, each curve represents the error convergence of each energy group.

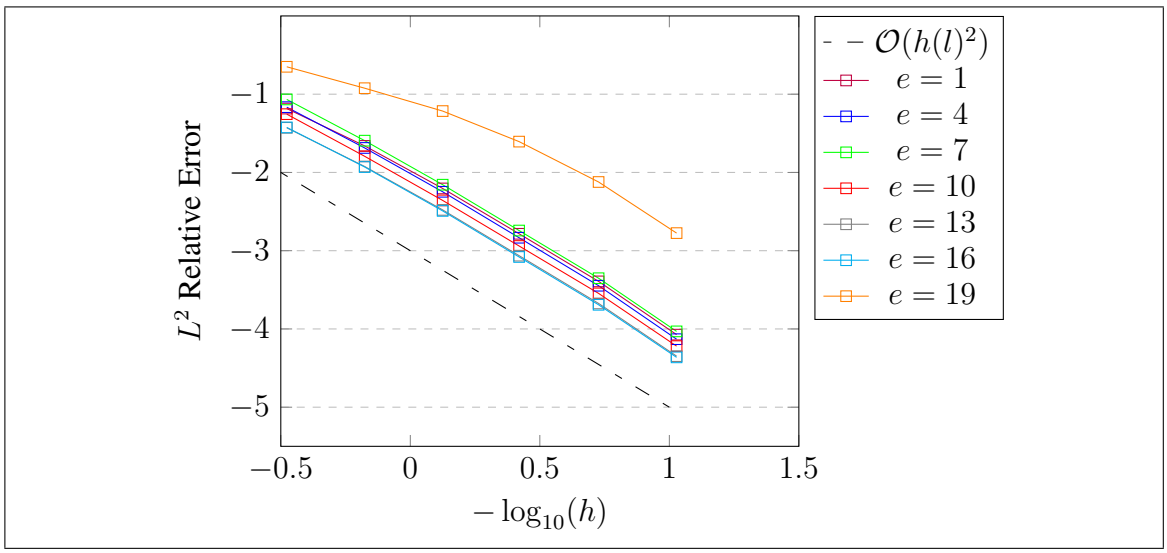

Figure 7.2. L^2 relative error between the discrete solution $\tilde{u}_l^{(e)}(\mathbf{x})$ and a fine-mesh solution: $\tilde{u}_7^{(e)}(\mathbf{x})$. The convergence of the first energy groups is $\mathcal{O}(h(l)^2)$. The last one reaches this convergence order when the mesh is fine enough.

We can see again that the error is converging for all energy groups and is highest for the last one.

The computed solution is shown in Figure 7.4 where we plot the sum of groups 1-3 as the fast neutron flux, the sum of groups 4-18 as the epithermal flux, and the sum of groups 19-20 as the thermal flux. This figure shows that the fast and epithermal fluxes are concentrated near the source, whereas the thermal flux peaks in the region between the lead and the source. The thermal flux in the source region is very small because the source material, Pu-240, is a strong absorber of thermal neutrons.

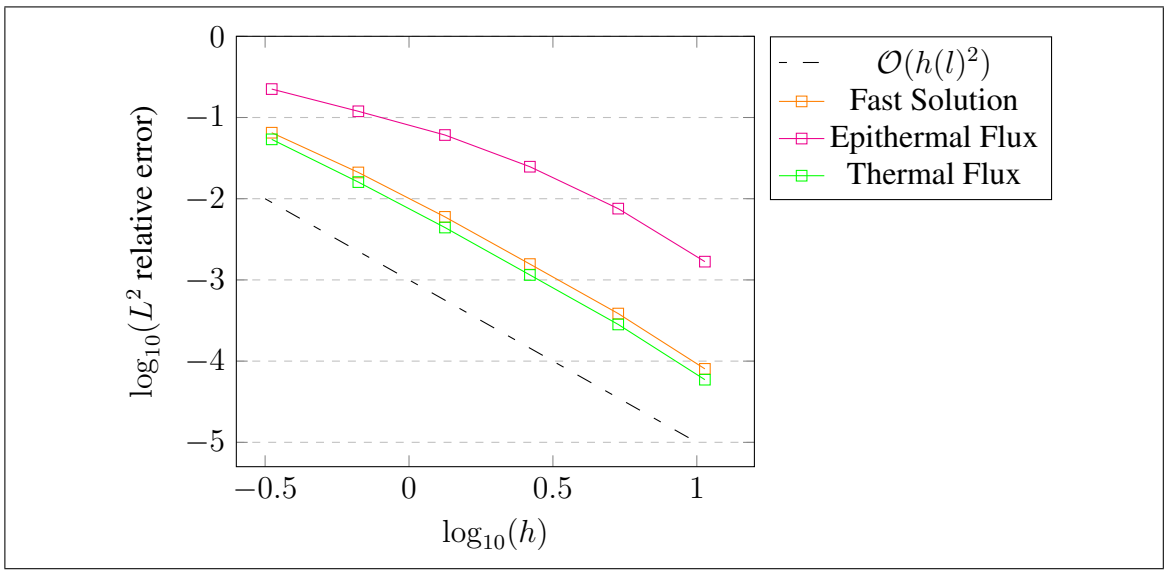

Figure 7.3. L^2 relative error between the discrete solution $\tilde{u}_l^{(e)}(\mathbf{x})$ and $\tilde{u}_7^{(e)}(\mathbf{x})$, for $l = \{1, 2, ..., 6\}$.

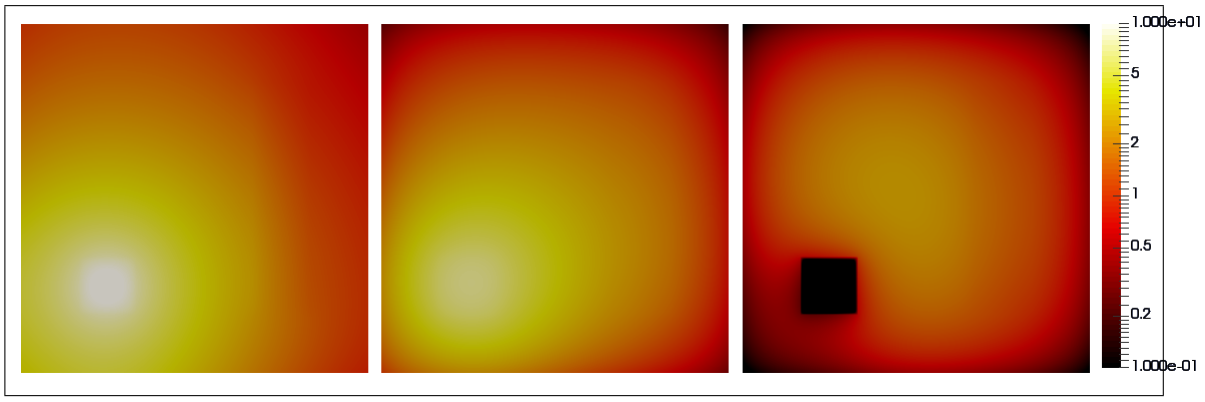

Figure 7.4. $\tilde{u}_7(\mathbf{x})$ discrete solution for fast solution (groups 1-3), epithermal flux (4-18) and thermal flux(19-20). The plot uses a logarithmic color scale.

7.4. Second Moment Results and Convergence

We computed the solution of seven discretization levels for the sparse tensor and five energy groups using full tensor; we compute the error between each level with the highest one: sparse tensor level 7.

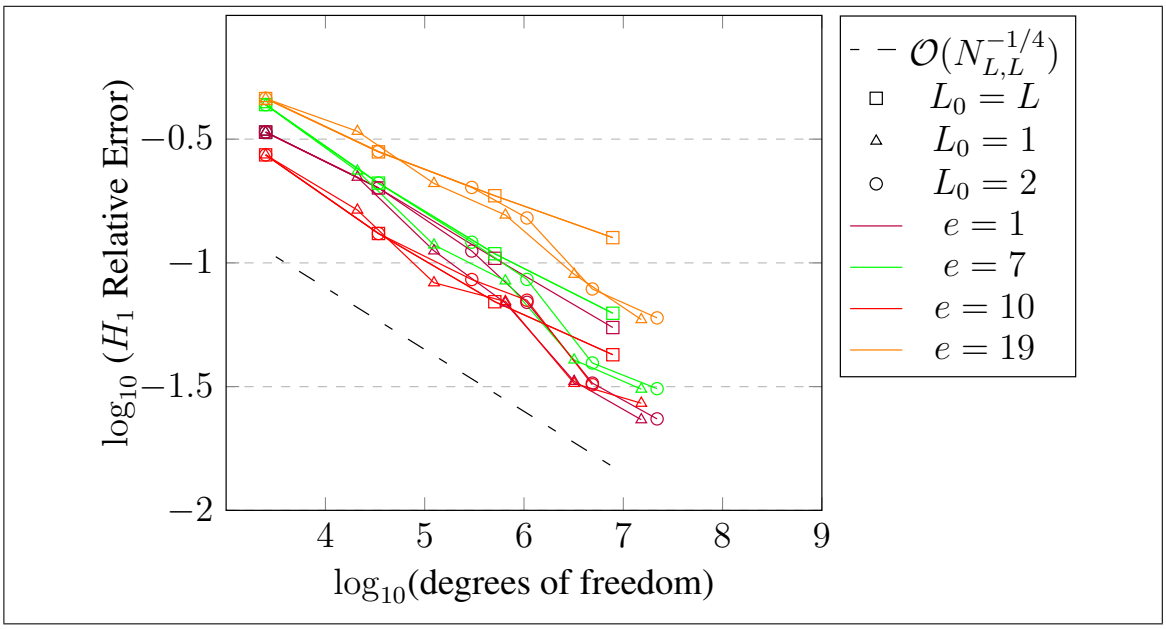

Figure 7.5. Convergence of the error in the sparse and full tensor solution for the second moment. We can see that the convergence of the first energy group using the full tensor is similar to $\mathcal{O}(N_{L,L}^{-1/4})$, which is the same as $\mathcal{O}(h(L))$.

The error convergence is shown in Figure 7.5. In this plot, we can compare the error between sparse tensor and full tensor for each energy group. These results indicate that the sparse tensor method does require fewer degrees of freedom to reach the same error level.

We also want to compare the errors of the sparse and full tensor with Monte Carlo. To do this, we generate samples of the source with a multivariate normal with the mean of the

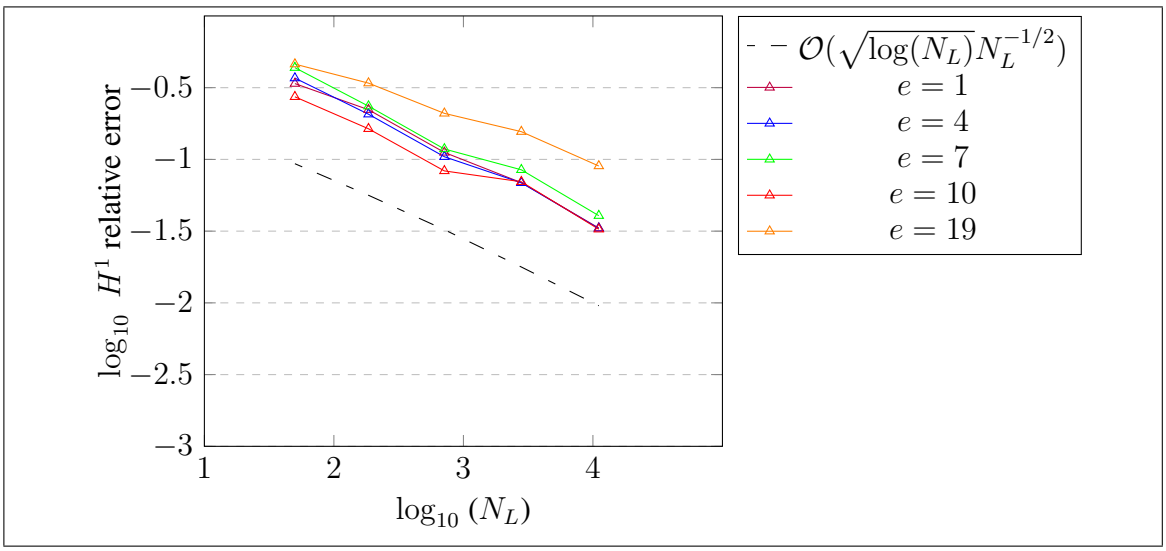

Figure 7.6. H^1 relative error between the discrete solution $U^{(ee)}_{L,L_0}(\mathbf{x},\mathbf{x})$ and the analytic solution $U^{(ee)}(\mathbf{x},\mathbf{x})$ for $e = \{1,2,3,4\}$, $L = \{1,2,...,5\}$. The discrete solution was obtained using Sparse Tensor with $L_0 = 1$. The convergence is like $\mathcal{O}(\sqrt{\log(N_L)}N_L^{-1/2})$.

source that we used for the first moment problem problem and the covariance that we used to compute the second moment. The results from 4 different Monte Carlo simulations are shown in Figure 7.7. In this figure the results of averaging the solution from different samples of the source for four different sets of samples are compared with the sparse tensor computation with 7 levels. These results indicate that the Monte Carlo computed second moment is converging to the deterministic value at a rate of the number of samples raised to the one-half power, as expected.

The computed solution of $\mathbb{E}[U_7(\mathbf{x},\mathbf{x})^{(e_1,e_2)}]$ using the sparse tensor approximations in Figure 7.8 for three different energy groups. In this figure we see that the second-moment is largest in the highest energy group inside the source region. Additionally, the second-moment is large in the middle of the problem for the low energy groups (in this case group 19); this can be physically explained because this region is expected to have the most downscattering to thermal energies.

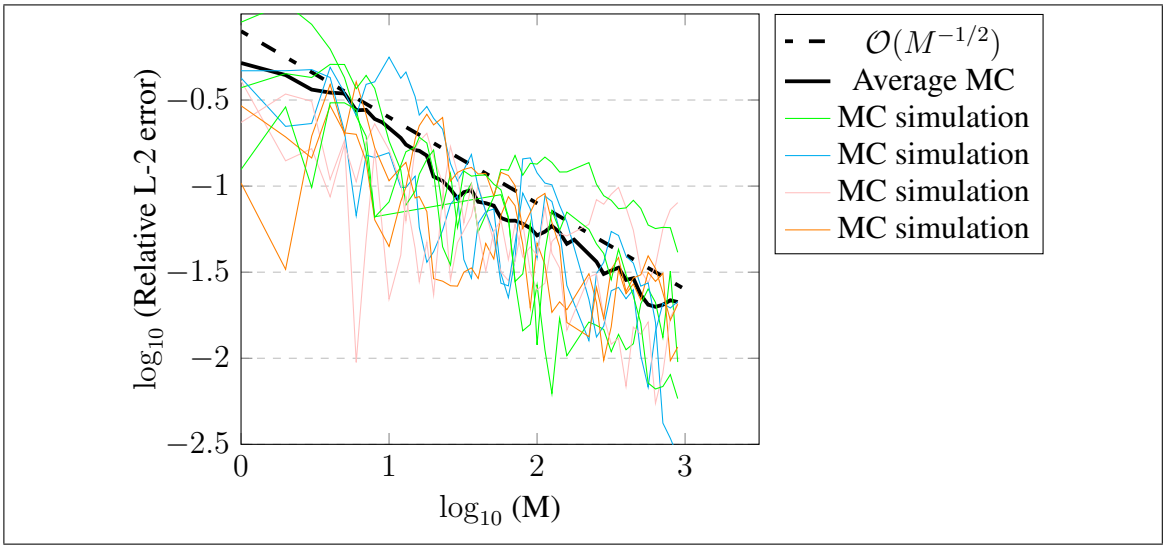

Figure 7.7. Comparison of error from a Monte Carlo simulation of the source uncertainty: the colored lines represents different Monte Carlo simulation. Each curve show the error between the average solution until iteration M and the the discrete solution $\hat{U}_{L,L_0}(\mathbf{x},\mathbf{x})$ with $L = 7$ and $L_0 = 2$. The black curve shows the average of the error of all the simulations. We can see that the average converges to the solution as $\mathcal{O}(M^{-1/2})$.

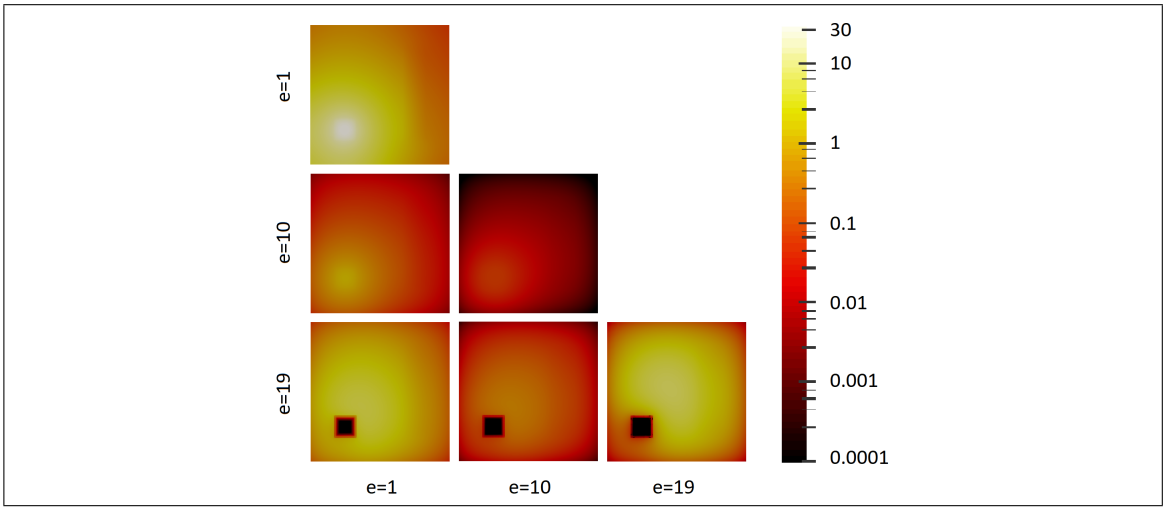

Figure 7.8. $U^{(e_1 e_2)}_{L,L_0}(\mathbf{x},\mathbf{x})$ obtained using the sparse tensor method with $L = 7$ $L_0 = 2$. Each plot represents the solution between two different energy groups. The plot uses a logarithmic color scale.

8. UNCERTAINTY IN THE σ PARAMETERS

In sections 3 to 7 we assumed the cross-sections, i.e., the σ's, were deterministic parameters. However, the cross section parameters are actually only known up to a non-negligible uncertainty. This uncertainty stems from the both the way measurements of the cross-sections are made and the processing that leads to the group-averaged cross-sections (Stacey, 2007; Zheng & McClarren, 2016, 2015). Indeed, what we have computed so far as the first and second moment is a conditional expectation, i.e., we have computed $\mathbb{E}[\tilde{u}^{(e_1e_2)}(\mathbf{x},\mathbf{y})|\theta]$ and $\mathbb{E}[U^{(e_1e_2)}(\mathbf{x},\mathbf{y})|\theta]$ where $\theta = \{\sigma_t^{e_1\to e_2}, \sigma_a^e, \sigma_s^e\}_{e,e_1,e_2=1}^{N_e}$. However, we want to compute $\mathbb{E}[\tilde{u}^{(e_1e_2)}(\mathbf{x},\mathbf{y})]$ and $\mathbb{E}[U^{(e_1e_2)}(\mathbf{x},\mathbf{y})]$ To achieve this, we must integrate over all the possible values of σ, without having to solve an arbitrary number of multigroup diffusion problems.

To this end, we need to find an efficient way to estimate the value of

$$\mathbb{E}[U^{(e_1e_2)}(\mathbf{x},\mathbf{y})] = \int_\Omega U^{(e_1e_2)}(\mathbf{x},\mathbf{y})\mathbb{P}(\theta(\omega))d\omega \tag{8.1}$$

In this section we are going to use the homogeneous problem considering just four energy groups and the parameters shown in Table C.1. We focus our attention on the computing of equation (8.1) just for $e_1 = e_2 = 0$ and $\mathbf{x} = \mathbf{y}$, to do the analysis. The same process could be done for all the energy groups.

Table 8.1. Removal cross section and diffusion coefficient for each energy group for water.

Energy Group	$\log_{10}\sigma_r$	$\log_{10} D^{(e)}$
1	-1.91582	0.60977
2	-1.33449	-0.21631
3	-1.29211	-0.24872
4	-2.26823	-0.44931

Table 8.2. Table of $\sigma_s^{\hat{e}\to e}$ for water. The rows are the initial energy group and the columns are the final energy group. Notice there is upscattering from group 4 to 3.

$$\begin{pmatrix} 1.39\times10^{-1} & 1.73\times10^{-3} & 1.28\times10^{-5} & 8.08\times10^{-8} \\ 0 & 1.32 & 4.59\times10^{-2} & 3.46\times10^{-4} \\ 0 & 0 & 1.44 & 5.06\times10^{-2} \\ 0 & 0 & 5.35\times10^{-4} & 1.74 \end{pmatrix}$$

To describe the randomness of the parameters, we are going to use the values given by Table 8.1 as mean values ($\bar{\theta}_i$) and the distribution of the parameters is given by,

$$\theta_i \sim \mathcal{U}(0.8\bar{\theta}_i, 1.2\bar{\theta}_i).$$

This is a wide uncertainty for the parameters chosen to be conservative.

8.1. Local Sensitivity Analysis

Firstly, we choose the parameters with higher sensitivity index for each energy group. This index measures how a little change in the parameter affects the solution, and is given by,

$$\mathrm{SI}_i = \sigma_i \frac{\partial Q}{\partial \theta_i}, \tag{8.2}$$

where σ_i is the standard deviation of the parameter i and Q is a quantity of interest, which in this case is given by $\mathbb{E}[\tilde{u}^{(ee)}(\mathbf{x},\mathbf{x})|\theta]$. We estimate the derivatives as

$$\frac{\partial Q}{\partial \theta_i}\Big| = \frac{Q(\bar{\theta}+\delta_i\hat{e}_i) - Q(\bar{\theta})}{\delta_i}.$$

This formulation will require the solution of $p+1$ multigroup diffusion problems to compute p sensitivities. For our 4 group problem there are $p = 24$ nonzero cross-sections.

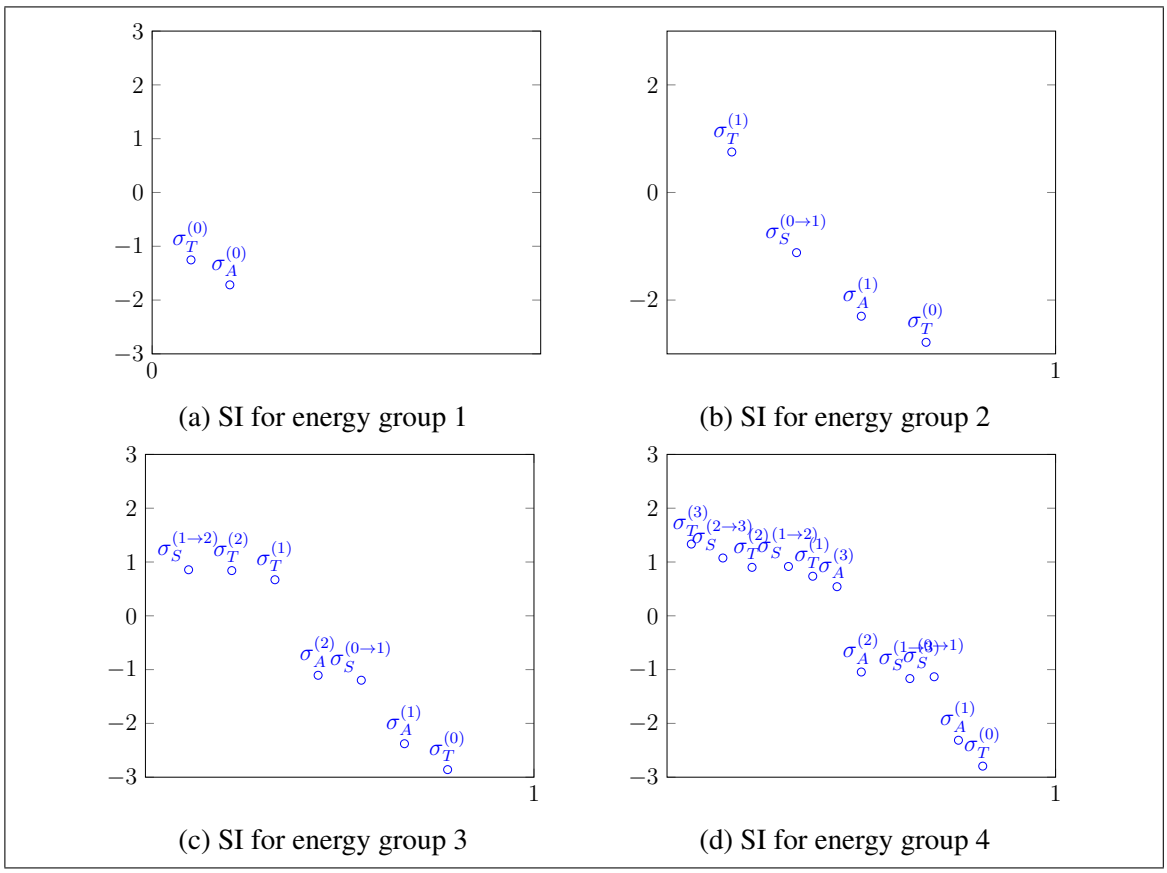

(a) SI for energy group 1

(b) SI for energy group 2

(c) SI for energy group 3

(d) SI for energy group 4

Figure 8.1. Local Sensitivity Indices of each parameter using as quantity of interest the $u_6^{(e)}(\mathbf{x}, \theta)$ for $e = \{1, 2, 3, 4\}$.

We can see in Figure 8.1 that for energy group 1, there are only two parameters affecting the solution. This could be explained because there is no scattering into group one. Thus, a change in the parameters of other groups doesn't change the solution of this. On the contrary, for energy group 4 all SI are different from 0, so a change in any parameter affects the solution of group 4. We can also see that in general the magnitude of the SI of groups 3 and 4 are higher the the SI of groups 1 and 2. Therefore we can say that the solution in lower energy levels is more sensible to changes on the parameters.

For the first energy group, we will integrate over the more significant parameters according to the SI shown in Figure 8.1(a).

8.2. Smolyak Quadratures

If we want to use a conventional quadrature rule to integrate a d-dimensional function, we need to compute

$$\int f(x_1, x_2, \ldots, x_d)dx \approx Q_l^{(d)}(f)$$
$$= \sum_{i_1=1}^{n_l} \sum_{i_2=1}^{n_l} \ldots \sum_{i_n=1}^{n_l} \omega_{l_{i_1}} \omega_{l_{i_2}} \ldots \omega_{l_{i_d}} f(x_{l_{i_1}}, \ldots, x_{l_{i_d}}) \quad (8.3)$$

which means that we need to evaluate the function in $(n_l)^d$ points. In our case, each value of the function is hard compute, so we use sparse grids to have a good approximation of the integral using less values of the function.

Given a level $\tilde{l} \in \mathbb{N}$ and a d-dimentional function f, the Smolyak construction is given by

$$S_l^d(f) = \sum_{l \leq |\mathbf{k}|_1 \leq l+d-1} (-1)^{l+d-|\mathbf{k}|_1-1} \binom{d-1}{|\mathbf{k}|_1 - l} (Q_{k_1}^1 \otimes Q_{k_2}^1 \otimes \ldots \otimes Q_{k_d}^1) f \quad (8.4)$$

(Gerstner & Griebel, 1998). When $d = 2$, the points of the sparse grid are shown in Figure 8.2 (Ayres & Eaton, 2015).

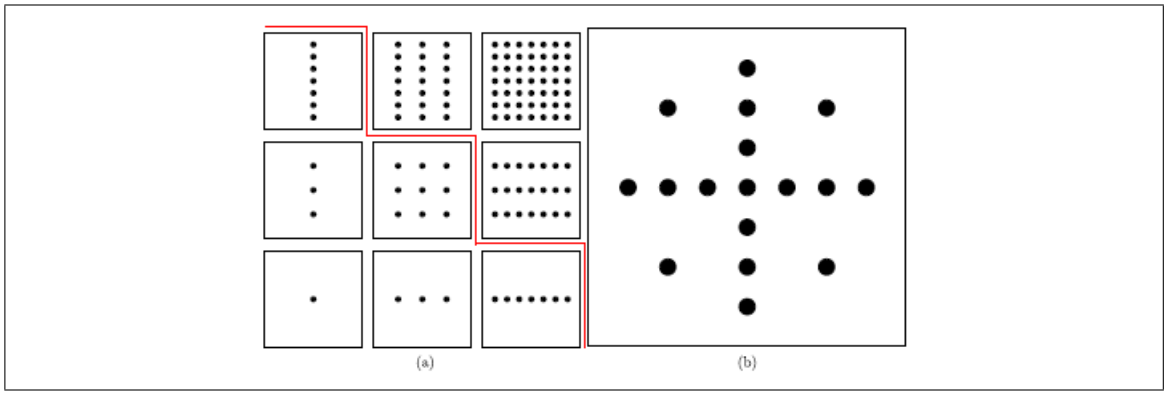

Figure 8.2. Sparse grid for $d = 2$ and $l = 3$

We used Gauss-Patterson quadrature rule to choose the points x_i and the weights ω_i (Burden & Faires, 2010).

8.3. Results and Convergence

We used discretization level 6 to do the integration. So, for each energy group, we are going to estimate,

$$\int_{\hat{\Omega}_e} \mathbb{E}[\tilde{u}_6^{(e)}(\mathbf{x})|\hat{\theta}_e]dP_{\hat{\theta}_e} \tag{8.5}$$

and

$$\int_{\hat{\Omega}_e} \mathbb{E}[U_6^{(ee)}(\mathbf{x},\mathbf{x})|\hat{\theta}_e]dP_{\hat{\theta}_e} \tag{8.6}$$

We are going to use sparse and full grids for different values of $\tilde{l}$ and compare the results with the one obtained using full grid with $\tilde{l} = 4$.

8.4. Results for the first energy group

For the first energy group, there are only two parameters with a sensitivity index different from 0. Thus, $\hat{\theta}_0 = (\sigma_T^{(0)}, \sigma_A^{(0)})$ and we integrate over this two parameters. In Figure 8.1 we can see the L^2 error between each level $\tilde{l}$ and the higher computed $(\tilde{l} = 4)$ using Smolyak Quadratures and Full Quadratures.

As we can see in fig:smolyak, using sparse grids we can have low errors between each quadrature degree $\tilde{l}$ and the higher one, computing much less values of $\tilde{u}_6(\mathbf{x})$ than using full grids. The same happens when computing the integral of the second moment for the discrete sparse and full tensor solution. For the other energy groups we might expect similar results.

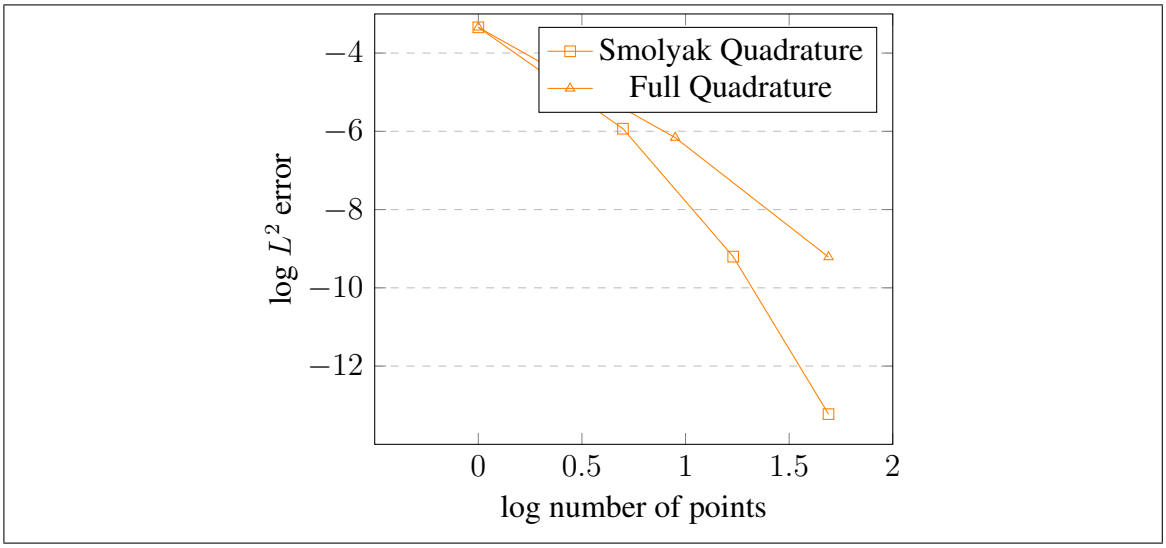

Figure 8.3. L^2 error between the integral estimation $Q_{\tilde{l}}(u_6^{(0)}(\mathbf{x},\omega))$ for each quadrature degree $\tilde{l}$ and the higher one computed ($\tilde{l}=4$). The squares shows the results using sparse grids and the triangles using full grids. For sparse grids, the number of points needed to estimate the integral value are lower.

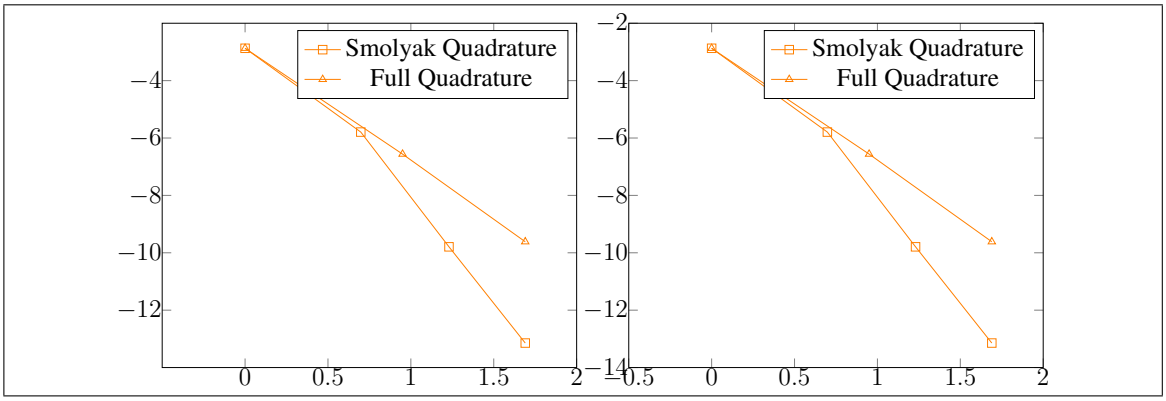

Figure 8.4. L^2 error between the integral estimation $Q_{\tilde{l}}(U_6^{(0)}(\mathbf{x},\omega))$ for each quadrature degree $\tilde{l}$ and the higher one computed ($\tilde{l}=4$). We have two plots, because the one of the right shows the convergence for the sparse tensor discrete solution, and the one of the left shows the convergence for the full tensor discrete solution.

9. CONCLUSIONS

In this work we presented an efficient method to quantify the uncertainty in the neutron flux due to the uncertainty in the parameters and in the source.

To do this, we first assumed the parameters as deterministic and compute an approximate discrete solution using FEM. We did this for both, the first and second moment. However, as the parameters are stochastic, we used full and sparse grids to estimate the value of the expectancy in the parameters.

In other words, what we wanted to estimate was $\mathbb{E}(\tilde{u}^{(e)}(\mathbf{x},\theta))$ and $\mathbb{E}(U^{(e)}(\mathbf{x},\mathbf{x},\theta))$. This was done computing $Q_{\tilde{l}}(\tilde{u}_l^{(e)}(\mathbf{x},\theta))$ and $Q_{\tilde{l}}(U_l^{(e)}(\mathbf{x},\mathbf{x},\theta))$, where l is the discretization level and $\tilde{l}$ is the quadrature degree. We want to ensure low errors for the first and second moment given by,

$$Error_{FM} := ||\mathbb{E}(\tilde{u}^{(e)}(\mathbf{x},\theta)) - Q_{\tilde{l}}(\tilde{u}_l^{(e)}(\mathbf{x},\theta))||_{L^2} \tag{9.1}$$

$$Error_{SM} := ||\mathbb{E}(U^{(ee)}(\mathbf{x},\theta)) - Q_l(U_l^{(ee)}(\mathbf{x},\mathbf{x},\theta))||_{L^2} \tag{9.2}$$

Using the triangular inequality we can bound the error as follows,

$$||\mathbb{E}(\tilde{u}^{(e)}(\mathbf{x},\theta)) - Q_{\hat{l}}(\tilde{u}_l^{(e)}(\mathbf{x},\theta))||_{L^2} \leq ||\mathbb{E}[\tilde{u}^{(e)}(\mathbf{x},\theta)) - u_l^{(e)}(\mathbf{x},\theta)]||_{L^2} + ||\mathbb{E}(u_l^{(e)}(\mathbf{x},\theta)) - Q_{\hat{l}}(\tilde{u}_l^{(e)}(\mathbf{x},\theta))||_{L^2} \tag{9.3}$$

$$||\mathbb{E}(U^{(e)}(\mathbf{x},\mathbf{x},\theta)) - Q_{\hat{l}}(U_l^{(e)}(\mathbf{x},\mathbf{x},\theta))||_{L^2} \leq ||\mathbb{E}[U^{(e)}(\mathbf{x},\mathbf{x},\theta)) - U_l^{(e)}(\mathbf{x},\mathbf{x},\theta)]||_{L^2} + ||\mathbb{E}[U_l^{(e)}(\mathbf{x},\mathbf{x},\theta)] - Q_{\hat{l}}[U_l^{(e)}[\mathbf{x},\mathbf{x},\theta]]||_{L^2} \tag{9.4}$$

We can see that the error depends on two approximations: first the discrete approximation of the function using FEM, and second, the integral approximation using quadratures.

The first term of the bound was studied on Section 6 and Section 7 and the second on Section 8. We focused our attention not just on achieving a low error, but also on computing a problem with less degrees of freedom.

For the second moment, the use of sparse tensor allows us to have low errors between the continious ans discrete solution ($||U^{(e)}(\mathbf{x},\mathbf{x},\theta) - U_l^{(e)}(\mathbf{x},\mathbf{x},\theta)||_{L^2}$) without dealing with the curse of dimensionality. On the other hand, for the first and second moment, using quadrature with sparse grids allows us to have low errors between the integral and the quadrature approximation ($||\mathbb{E}[u_l^{(e)}(\mathbf{x},\theta)] - Q_{\hat{l}}(\tilde{u}_l^{(e)}(\mathbf{x},\theta))||_{L^2}$ and $||\mathbb{E}[U_l^{(e)}(\mathbf{x},\mathbf{x},\theta)] - Q_{\hat{l}}(U_l^{(e)}(\mathbf{x},\mathbf{x},\theta))||_{L^2}$), evaluating the function in less points than full grids.

Only if we are able to achieve low errors in the two approximation process we will have a good estimation of the quantity of interest we are interested in. The high dimensionality of this problem encouraged us to use efficient methods as Sparse Tensor and Smolyak Quadratures, and they showed a good performance in this field.

REFERENCES

Ayres, D., & Eaton, M. (2015). Uncertainty quantification in nuclear criticality modelling using a high dimensional model representation. *Annals of Nuclear Energy*, *80*(Complete), 379-402.

Beddek, K., Le Menach, Y., Clenet, S., & Moreau, O. (2011, May). 3-d stochastic spectral finite-element method in static electromagnetism using vector potential formulation. *Magnetics, IEEE Transactions on*, *47*(5), 1250-1253.

Bell, G. I., & Glasstone, S. (1970). *Nuclear reactor theory*. Malabar, Florida: Robert E. Kreiger Publishing.

Bourhrara, L. (2006). H1 approximations of the neutron transport equation and associated diffusion equations. *Transport Theory and Statistical Physics*, *35*(3-4), 89-108.

Brunner, T. A., Mehlhorn, T., McClarren, R. G., & Kurecka, C. J. (2005). Advances in radiation modeling in alegra: A final report for ldrd-67120, efficient implicit multigroup radiation calculations. *Sandia National Laboratories*.

Burden, R., & Faires, J. (2010). *Numerical analysis*. Cengage Learning.

Dashti, M., & Stuart, A. (2016). The Bayesian approach to inverse problems. *Handbook of UQ (R. Ghanem etal., Eds.)*.

Du, Y., Luo, Y., & Kong, J.-A. (2008, Oct). Electromagnetic scattering from randomly rough surfaces using the stochastic second-degree method and the sparse matrix/canonical grid algorithm. *Geoscience and Remote Sensing, IEEE Transactions on*, *46*(10), 2831-2839.

Duerigen, S. (2013). *Neutron transport in hexagonal reactor cores modeled by trigonal-geometry diffusion and simplified p3 nodal methods* (Unpublished doctoral dissertation). Karlsruhe Institute of Technology, Germany.

Evans, J. (2015, March). *The diffusion approximation in neutron transport theory asymptotic expansions.* Department of Mathematical Science University of Bath.

Gerstner, T., & Griebel, M. (1998, Jan 01). Numerical integration using sparse grids.

Numerical Algorithms, *18*(3), 209.

Habetler, G. J., & Martino, M. A. (1961). Existence theorems and spectral theory for the multigroup diffusion model. In *Proc. Sympos. Appl. Math., Vol. XI* (pp. 127–139). American Mathematical Society, Providence, R.I.

Haidar, N. H. S. (1992). Nodal adjoint method for multigroup diffusion in heterogeneous slab reactors. *Numerical Methods for Partial Differential Equations*, *8*(6), 515-535.

Hanuš, M. (2011). *Mathematical modeling of neutron transport: Theoretical and computational point of view*. LAP LAMBERT Academic Publishing.

Hanuš, M., & McClarren, R. G. (2016). On the use of symmetrized transport equation in goal-oriented adaptivity. *Journal of Computational and Theoretical Transport*, *45*(4), 314–333.

Harbrecht, H. (2014). Second moment analysis for robin boundary value problems on random domains. In M. Griebel (Ed.), *Singular phenomena and scaling in mathematical models* (pp. 361–381). Cham: Springer International Publishing.

Harbrecht, H., Peters, M., & Siebenmorgen, M. (2013). Combination technique based k-th moment analysis of elliptic problems with random diffusion. *Journal of Computational Physics*, *252*, 128 - 141.

Harbrecht, H., Schneider, R., & Schwab, C. (2008). Sparse second moment analysis for elliptic problems in stochastic domains. *Numer. Math.*, *109*(3), 385–414.

Hasan, M. Z., & Conn, R. W. (1987). A two-dimensional finite element multigroup diffusion theory for neutral atom transport in plasmas. *Journal of Computational Physics*, *71*(2), 371 - 390.

Hauck, C. D., & McClarren, R. G. (2013). A collision-based hybrid method for time dependent, linear, kinetic transport equations. *Multiscale Modeling and Simulation*, *11*(4), 1197–1227.

Helmut Harbrecht, R. S., & Schwab, C. (2008). Sparse second moment analysis for elliptic problems in stochastic domains. *Numerische Matematik*, *109*(3), 385 - 414.

Hiptmair, R., Jerez-Hanckes, C., & Schwab, C. (2013). Sparse tensor edge elements. *BIT Numerical Mathematics*, *53*(4), 925–939.

Hosseini, S. A., & Saadatian-Derakhshandeh, F. (2015). Galerkin and generalized least squares finite element: A comparative study for multi-group diffusion solvers. *Progress in Nuclear Energy*, *85*, 473 - 490.

Jerez-Hanckes, C., & Schwab, C. (2017). Electromagnetic wave scattering by random surfaces: uncertainty quantification via sparse tensor boundary elements. *IMA Journal of Numerical Analysis*, *37*(3), 1175–1210.

Knupp, P., & Salari, K. (2002). *Verification of computer codes in computational science and engineering*. CRC Press.

Koeze, D. (2012). *Goal-oriented angular adaptive algorithm using sensitivity analysis for the transport equation and boltzmann-fokker-planck equation* (Unpublished doctoral dissertation). Delft University of Technology, Netherlands.

Lamarsh, J. R. (2001). *Introduction to nuclear reactor theory* (3rd ed.). Pearson.

Larsen, E., & Morel, J. (1989, 1). Asymptotic solutions of numerical transport problems in optically thick, diffusive regimes ii. *Journal of Computational Physics*, *83*(1), 212–236.

Lingus, C. (1971). Analytical test case's for neutron and radiation transport codes. In *Second conference on transport theory* (p. 655).

McClarren, R. G. (2017). *Computational nuclear engineering and radiological science using python*. Academic Press.

McClarren, R. G., Drake, R. P., Morel, J. E., & Holloway, J. P. (2010). Theory of radiative shocks in the mixed, optically thick-thin case. *Physics of Plasmas*, *17*, 093301.

McClarren, R. G., & Lowrie, R. B. (2008). Manufactured solutions for the p1 radiation-hydrodynamics equations. *Journal of Quantitative Spectroscopy and Radiative Transfer*, *109*(15), 2590–2602.

McClarren, R. G., Ryu, D., & Drake, R. P. (2010). A physics informed emulator for laser-driven radiating shock simulations. *Reliability Engineering and System Safety*, *96*(9), 1194–1207.

McClarren, R. G., & Wohlbier, J. G. (2010). Analytic solutions for ion-electron-radiation coupling with radiation and electron diffusion. *Journal of Quantitative Spectroscopy*

and Radiative Transfer, *112*, 119–130.

Myneni, R. B., Radiative, G. A. J. o. Q. S., , & 1993. (1993, June). Radiative transfer in three-dimensional atmosphere-vegetation media. *Elsevier*, *49*(6), 585–598.

Sanchez, R., & McCormick, N. J. (1982). A review of neutron transport approximations. *Nuclear Science and Engineering*, *80*(4), 481-535.

Saracco, P., Dulla, S., & Ravetto, P. (2012). On the spectrum of the multigroup diffusion equations. *Progress in Nuclear Energy*, *59*, 86 - 95.

Schwab, C., Süli, E., & Todor, R. A. (2008). Sparse finite element approximation of high-dimensional transport-dominated diffusion problems. *M2AN Math. Model. Numer. Anal.*, *42*(5), 777–819.

Schwab, C., & Todor, R. A. (2006). Karhunen-Loève approximation of random fields by generalized fast multipole methods. *J. Comput. Phys.*, *217*(1), 100–122.

Stacey, W. (2007). *Nuclear reactor physics*. John Wiley & Sons.

Steinbach, O. (2007). *Numerical approximation methods for elliptic boundary value problems: Finite and boundary elements*. Springer New York.

Stewart, H. (1974, September). *Properties of solutions and eigenfunctions of multigroup diffusion problems* (Tech. Rep. No. 2048). Institut für Neutronenphysik und Reaktortechnik.

Stewart, H. (1976). Spectral theory of heterogeneous diffusion systems. *Journal of Mathematical Analysis and Applications*, *54*(1), 59 - 78.

von Petersdorff, T., & Schwab, C. (2006). Sparse finite element methods for operator equations with stochastic data. *Appl. Math.*, *51*(2), 145–180.

Wang, Y., & Ragusa, J. (2009). Application of hp adaptivity to the multigroup diffusion equations. *Nuclear Science and Engineering*, *161*(1), 22-48.

Zheng, W., & McClarren, R. G. (2015). Semi-analytic benchmark for multi-group free-gas legendre moments and the application of gauss quadrature in generating thermal scattering legendre moments. *Annals of Nuclear Energy*, *85*, 1131–1140.

Zheng, W., & McClarren, R. G. (2016). Emulation-based calibration for parameters in parameterized phonon spectrum of zrh x in triga reactor simulations. *Nuclear*

science and engineering, *183*(1), 78–95.

Zwermann, W., Aures, A., Gallner, L., Hannstein, V., Krzykacz-Hausmann, B., Velkov, K., & Martinez, J. (2014). Nuclear data uncertainty and sensitivity analysis with XSUSA for fuel assembly depletion calculations. *Nuclear Engineering and Technology*, *46*(3), 343-352.

APPENDICES

APPENDIX A. PROOF THEOREM 5.1

PROOF. Assuming down-scattering, i.e. $\mathcal{B}^{(e\hat{e})} \equiv 0$ for $\hat{e} \geq e$. For any $v_h^{(e)} \in V_h$, Galerkin orthogonality between (3.7) and its discrete counterpart yields

$$a^{(e)}\left(u^{(e)} - u_h^{(e)}, v_h^{(e)}\right) = \sum_{\hat{e}=1}^{e-1} b^{(e\hat{e})}\left(u^{(\hat{e})} - u_h^{(\hat{e})}, v_h^{(e)}\right). \tag{A.1}$$

By continuity and ellipticity of $A^{(e)}$, we derive

$$\begin{aligned} c_1^{A^{(e)}}\|u^{(e)} - u_h^{(e)}\|_{H^1}^2 &\leq a^{(e)}\left(u^{(e)} - u_h^{(e)}, u^{(e)} - u_h^{(e)}\right) \\ &\leq c_2^{A^{(e)}}\|u^{(e)} - u_h^{(e)}\|_{H^1}\|u^{(e)} - v_h^{(e)}\|_{H^1} \\ &\quad + \sum_{\hat{e}=1}^{e-1}\|\sigma_s^{(\hat{e}\to e)}\|_{L^\infty}\|u^{(\hat{e})} - u_h^{(\hat{e})}\|_{L^2}\,\|v_h^{(e)} - u_h^{(e)}\|_{L^2} \end{aligned}$$

After rearranging terms, one can obtain

$$\|u^{(e')} - u_h^{(e')}\|_{H^1} \leq \frac{c_2^{A^{(e)}}}{c_1^{A^{(e)}}} \inf_{v_h^{(e)} \in V_h} \|u^{(e)} - v_h^{(e)}\|_{H^1} + \frac{2}{c_1^{A^{(e)}}} \sum_{\hat{e}=1}^{e-1}\|\sigma_s^{(\hat{e}\to e)}\|_{L^\infty}\,\|u^{(\hat{e})} - u_h^{(\hat{e})}\|_{L^2} \tag{A.2}$$

Equation (A.2) holds for every $e \geq 2$. We will use this inequality to prove the theorem by induction. For $e = 2$ we have,

$$\begin{aligned} \|u^{(2)} - u_h^{(2)}\|_{L^2} \leq \|u^{(2)} - u_h^{(2)}\|_{H^1} &\leq \frac{c_2^{A^{(2)}}}{c_1^{A^{(1)}}} \inf_{v_h^{(2)} \in V_h} \|u^{(2)} - v_h^{(2)}\|_{H^1} && \text{(A.3)} \\ &\quad + \frac{2}{c_1^{A^{(2)}}}\|\sigma_s^{(1\to 2)}\|_\infty\,\|u^{(1)} - u_h^{(1)}\|_{L^2} && \text{(A.4)} \\ &\leq C^{(2)} + \frac{2}{c_1^{A^{(2)}}}\|\sigma_s^{(1\to 2)}\|_\infty\,\|u^{(1)} - u_h^{(1)}\|_{L^2} && \text{(A.5)} \end{aligned}$$

We assumed (5.13) holds for $e = e_0$ and now we need to prove that the statement holds for $e = e_0 + 1$,

$$
\begin{aligned}
& \|u^{(e_0+1)} - u_h^{(e_0+1)}\|_{H^1} \\
\leq\ & \frac{c_2^{A^{(e_0+1)}}}{c_1^{A^{(e_0+1)}}} \inf_{v_h^{(e_0+1)} \in V_h} \|u^{(e_0+1)} - v_h^{(e_0+1)}\|_{H^1} \\
& + \frac{2}{c_1^{A^{(e_0+1)}}} \sum_{e'=1}^{e_0} \|\sigma_s^{(e' \to e_0+1)}\|_\infty \, \|u^{(e')} - u_h^{(e')}\|_{L^2} \\
\leq\ & \frac{c_2^{A^{(e_0+1)}}}{c_1^{A^{(e_0+1)}}} \inf_{v_h^{(e_0+1)} \in V_h} \|u^{(e_0+1)} - v_h^{(e_0+1)}\|_{H^1} \\
& + \frac{2}{c_1^{A^{(e_0+1)}}} \sum_{e'=1}^{e_0-1} \|\sigma_s^{(e' \to e_0+1)}\|_\infty \, \|u^{(e')} - u_h^{(e')}\|_{L^2} \\
& + \frac{2}{c_1^{A^{(e_0+1)}}} \|\sigma_s^{(e_0 \to e_0+1)}\|_\infty \, \|u^{(e_0)} - u_h^{(e_0)}\|_{L^2} \\
\leq\ & \frac{c_2^{A^{(e_0+1)}}}{c_1^{A^{(e_0+1)}}} \inf_{v_h^{(e_0+1)} \in V_h} \|u^{(e_0+1)} - v_h^{(e_0+1)}\|_{H^1} + \\
& \frac{2}{c_1^{A^{(e_0+1)}}} \sum_{e'=1}^{e_0-1} \|\sigma_s^{(e' \to e_0+1)}\|_\infty \, \|u^{(e')} - u_h^{(e')}\|_{L^2} \\
& + \frac{2\|\sigma_s^{(e_0 \to e_0+1)}\|_\infty}{c_1^{A^{(e_0+1)}}} \left(C^{(e_0)} + \prod_{e=1}^{e_0-1} \frac{2}{c_1^{A^{(e+1)}}} \|\sigma_s^{(e \to e+1)}\|_\infty \|u^{(1)} - u_h^{(1)}\|_{L^2} \right) \\
\leq\ & C^{(e_0+1)} + \frac{2\|\sigma_s^{(e_0 \to e_0+1)}\|_\infty}{c_1^{A^{(e_0+1)}}} \prod_{e=1}^{e_0-1} \frac{2}{c_1^{A^{(e+1)}}} \|\sigma_s^{(e \to e+1)}\|_\infty \|u^{(1)} - u_h^{(1)}\|_{L^2} \\
\leq\ & C^{(e_0+1)} + \prod_{e=1}^{e_0} \frac{2}{c_1^{A^{(e+1)}}} \|\sigma_s^{(e \to e+1)}\|_\infty \|u^{(1)} - u_h^{(1)}\|_{L^2}
\end{aligned}
$$

As L^2-norm is less or equal to H^1-norm,

$$
\|u^{(e_0+1)} - u_h^{(e_0+1)}\|_{L^2} \ \leq\ C^{(e_0+1)} + \prod_{e=1}^{e_0} \frac{2}{c_1^{A^{(e+1)}}} \|\sigma_s^{(e \to e+1)}\|_\infty \|u^{(1)} - u_h^{(1)}\|_{L^2}
$$

By induction, equation (5.13) is true for any $N \in \{1, ..., N_E\}$ □

APPENDIX B. SCATTERING CROSS SECTION

Table B.1. σ_s values

$(e, \hat{e})$	$\mathcal{D}_s$	$\mathcal{D}_a$	$\mathcal{D}_b$
(0,0)	0.134	0.159	0.0396
(0,1)	0.011	0.022	0.026
(0,2)	0.0081	0.052	0.0152
(0,3)	0.0127	0.066	0.0093
(0,4)	0.0148	0.0425	0.0044
(0,5)	0.0107	0.0235	0.0021
(0,6)	0.0054	0.0099	0.00106
(0,7)	0.0022	0.00396	0.00055
(0,8)	0.00076	0.00158	0.000292
(0,9)	0.00026	0.00063	0.000156
(0,10)	0.000144	0.000354	0.00013
(0,11)	2.29e-05	5.7e-05	3.82e-05
(0,12)	3.68e-06	9e-06	1.12e-05
(0,13)	6.1e-07	1.45e-06	3.3e-06
(0,14)	1e-07	2.32e-07	9.7e-07
(0,15)	1.58e-08	3.7e-08	2.85e-07
(0,16)	1.95e-09	4.77e-09	8.4e-08
(0,17)	1.7e-10	4.48e-10	2.39e-08
(0,18)	0.0	0.0	3.05e-10
(0,19)	0.0	0.0	0.0
(1,1)	0.185	0.243	0.057
(1,2)	0.0115	0.0278	0.0374
(1,3)	0.0174	0.0499	0.0177
(1,4)	0.0187	0.0319	0.0105
(1,5)	0.0125	0.0156	0.0057
(1,6)	0.0061	0.0065	0.00302
(1,7)	0.00239	0.00219	0.00162
(1,8)	0.00084	0.00074	0.00086
(1,9)	0.000298	0.000266	0.000465
(1,10)	0.000165	0.000136	0.000387
(1,11)	2.64e-05	1.94e-05	0.000113
(1,12)	4.23e-06	2.88e-06	3.31e-05
(1,13)	7.1e-07	4.42e-07	9.7e-06
(1,14)	1.15e-07	6.9e-08	2.86e-06
(1,15)	1.83e-08	1.06e-08	8.4e-07
(1,16)	2.33e-09	1.67e-09	2.48e-07
(1,17)	2.33e-10	2.06e-10	7.3e-08
(1,18)	0.0	0.0	1.36e-08
(1,19)	0.0	0.0	0.0
(2,2)	0.211	0.397	0.091
(2,3)	0.0171	0.0099	0.053
(2,4)	0.0241	0.0148	0.0266
(2,5)	0.0191	0.0096	0.0145
(2,6)	0.0102	0.0041	0.0079
(2,7)	0.00419	0.00191	0.00427
(2,8)	0.00149	0.00081	0.00232
(2,9)	0.00053	0.000311	0.00126
(2,10)	0.000295	0.000142	0.00106
(2,11)	4.69e-05	1.4e-05	0.000311
(2,12)	7.5e-06	1.24e-06	9.1e-05
(2,13)	1.26e-06	1.11e-07	2.69e-05
(2,14)	2.02e-07	1.04e-08	7.9e-06
(2,15)	3.34e-08	8.9e-10	2.33e-06
(2,16)	4.75e-09	0.0	6.9e-07
(2,17)	4.64e-10	0.0	2.02e-07

$(e, \hat{e})$	$\mathcal{D}_s$	$\mathcal{D}_a$	$\mathcal{D}_b$
(6,6)	0.434	0.442	0.249
(6,7)	0.0185	0.00488	0.205
(6,8)	0.000158	0.0	0.1
(6,9)	4.38e-06	0.0	0.054
(6,10)	5.7e-08	0.0	0.0457
(6,11)	4.98e-09	0.0	0.0134
(6,12)	4.32e-10	0.0	0.00396
(6,13)	0.0	0.0	0.00116
(6,14)	0.0	0.0	0.000342
(6,15)	0.0	0.0	0.000101
(6,16)	0.0	0.0	2.97e-05
(6,17)	0.0	0.0	8.7e-06
(6,18)	0.0	0.0	3.54e-06
(6,19)	0.0	0.0	0.0
(7,7)	0.487	0.517	0.298
(7,8)	0.023	0.0059	0.262
(7,9)	2.57e-05	0.0	0.132
(7,10)	4.86e-06	0.0	0.11
(7,11)	2.14e-07	0.0	0.0325
(7,12)	1.51e-08	0.0	0.0096
(7,13)	1.31e-09	0.0	0.00282
(7,14)	1.14e-10	0.0	0.00083
(7,15)	0.0	0.0	0.000244
(7,16)	0.0	0.0	7.2e-05
(7,17)	0.0	0.0	2.11e-05
(7,18)	0.0	0.0	8.7e-06
(7,19)	0.0	0.0	0.0
(8,8)	0.53	0.618	0.352
(8,9)	0.0193	0.0071	0.322
(8,10)	0.0054	0.0	0.253
(8,11)	0.0	0.0	0.074
(8,12)	0.0	0.0	0.0219
(8,13)	0.0	0.0	0.0065
(8,14)	0.0	0.0	0.0019
(8,15)	0.0	0.0	0.00056
(8,16)	0.0	0.0	0.000164
(8,17)	0.0	0.0	4.84e-05
(8,18)	0.0	0.0	2e-05
(8,19)	0.0	0.0	0.0
(9,9)	0.559	0.6	0.398
(9,10)	0.0074	0.007	0.566
(9,11)	0.00116	0.0	0.161
(9,12)	0.000103	0.0	0.0473
(9,13)	9.1e-06	0.0	0.0139
(9,14)	7.9e-07	0.0	0.0041
(9,15)	6.8e-08	0.0	0.00121
(9,16)	6e-09	0.0	0.000355
(9,17)	5.3e-10	0.0	0.000104
(9,18)	5.8e-11	0.0	4.34e-05
(9,19)	0.0	0.0	0.0
(10,10)	0.541	0.628	0.712
(10,11)	0.00187	0.00256	0.443
(10,12)	0.0	0.0	0.128
(10,13)	0.0	0.0	0.0377
(10,14)	0.0	0.0	0.0111

Table B.2. σ_s values

$(e, \hat{e})$	$\mathcal{D}_s$	$\mathcal{D}_a$	$\mathcal{D}_b$
(2,18)	0.0	0.0	5.9e-08
(2,19)	0.0	0.0	0.0
(3,3)	0.191	0.312	0.114
(3,4)	0.0229	0.00287	0.081
(3,5)	0.0214	0.0	0.0381
(3,6)	0.0118	0.0	0.0207
(3,7)	0.00436	0.0	0.0112
(3,8)	0.00153	0.0	0.0061
(3,9)	0.00055	0.0	0.00332
(3,10)	0.000301	0.0	0.00278
(3,11)	4.76e-05	0.0	0.00082
(3,12)	7.6e-06	0.0	0.000241
(3,13)	1.28e-06	0.0	7.1e-05
(3,14)	2.03e-07	0.0	2.09e-05
(3,15)	3.38e-08	0.0	6.1e-06
(3,16)	5.4e-09	0.0	1.81e-06
(3,17)	7.3e-10	0.0	5.3e-07
(3,18)	8.4e-11	0.0	1.85e-07
(3,19)	0.0	0.0	0.0
(4,4)	0.232	0.277	0.187
(4,5)	0.0149	0.00258	0.112
(4,6)	0.0097	0.0	0.053
(4,7)	0.0066	0.0	0.0289
(4,8)	0.00261	0.0	0.0157
(4,9)	0.00072	0.0	0.0085
(4,10)	0.000285	0.0	0.0071
(4,11)	2.37e-05	0.0	0.0021
(4,12)	2.16e-06	0.0	0.00062
(4,13)	2.05e-07	0.0	0.000182
(4,14)	2.06e-08	0.0	5.4e-05
(4,15)	2.25e-09	0.0	1.58e-05
(4,16)	1.64e-10	0.0	4.64e-06
(4,17)	0.0	0.0	1.36e-06
(4,18)	0.0	0.0	5.2e-07
(4,19)	0.0	0.0	0.0
(5,5)	0.351	0.257	0.246
(5,6)	0.0138	0.00284	0.168
(5,7)	2.78e-06	0.0	0.073
(5,8)	0.000262	0.0	0.0399
(5,9)	0.000453	0.0	0.0217
(5,10)	0.000197	0.0	0.0182
(5,11)	2.31e-05	0.0	0.0053
(5,12)	2.55e-06	0.0	0.00157
(5,13)	3.8e-07	0.0	0.000463
(5,14)	6.3e-08	0.0	0.000136
(5,15)	6.2e-09	0.0	4.01e-05
(5,16)	5.7e-10	0.0	1.18e-05
(5,17)	7.1e-11	0.0	3.47e-06
(5,18)	0.0	0.0	1.38e-06

$(e, \hat{e})$	$\mathcal{D}_s$	$\mathcal{D}_a$	$\mathcal{D}_b$
(10,15)	0.0	0.0	0.00327
(10,16)	0.0	0.0	0.00096
(10,17)	0.0	0.0	0.000283
(10,18)	0.0	0.0	0.000118
(10,19)	0.0	0.0	7.6e-08
(11,11)	0.527	0.643	0.765
(11,12)	0.00191	0.00262	0.481
(11,13)	0.0	0.0	0.139
(11,14)	0.0	0.0	0.041
(11,15)	0.0	0.0	0.0121
(11,16)	0.0	0.0	0.00355
(11,17)	0.0	0.0	0.00104
(11,18)	0.0	0.0	0.000435
(11,19)	0.0	0.0	8e-07
(12,12)	0.459	0.647	0.783
(12,13)	0.0012	0.00264	0.493
(12,14)	0.0	0.0	0.143
(12,15)	0.0	0.0	0.0421
(12,16)	0.0	0.0	0.0124
(12,17)	0.0	0.0	0.00365
(12,18)	0.0	0.0	0.00152
(12,19)	0.0	0.0	3.37e-06
(13,13)	0.394	0.649	0.789
(13,14)	0.00105	0.00264	0.497
(13,15)	0.0	0.0	0.144
(13,16)	0.0	0.0	0.0425
(13,17)	0.0	0.0	0.0125
(13,18)	0.0	0.0	0.0052
(13,19)	0.0	0.0	1.21e-05
(14,14)	0.44	0.649	0.791
(14,15)	0.00153	0.00264	0.499
(14,16)	0.0	0.0	0.145
(14,17)	0.0	0.0	0.0426
(14,18)	0.0	0.0	0.0177
(14,19)	0.0	0.0	4.18e-05
(15,15)	0.277	0.649	0.791
(15,16)	0.000274	0.00265	0.499
(15,17)	0.0	0.0	0.145
(15,18)	0.0	0.0	0.06
(15,19)	0.0	0.0	0.000143
(16,16)	0.343	0.649	0.792
(16,17)	0.00128	0.00265	0.499
(16,18)	0.0	0.0	0.205
(16,19)	0.0	0.0	0.000487
(17,17)	0.56	0.649	0.794
(17,18)	0.00088	0.00265	0.705
(17,19)	0.0	0.0	0.00166
(18,18)	1.102	0.652	1.717
(18,19)	4.09e-07	1.51e-05	0.00405
(19,19)	0.05	0.693	4.362

APPENDIX C. REMOVAL CROSS SECTION AND DIFFUSION COEFFICIENTS

Table C.1. $\log_{10}$ values of removal cross section (σ_r), diffusion coefficient (D) and source value (μ) for each energy group and each subdomain. The numbers in parenthesis are the logarithm of the midpoint energy of each group in MeV.

	$\sigma_r^{(e)}$			$D^{(e)}$			
e	$\mathcal{D}_b$	$\mathcal{D}_a$	$\mathcal{D}_s$	$\mathcal{D}_b$	$\mathcal{D}_a$	$\mathcal{D}_s$	μ
1 (1.04)	-1.104	-0.435	-0.641	0.294	0.621	0.266	1.04
2 (0.774)	-1.087	-0.566	-0.621	0.253	0.506	0.23	0.774
3 (0.509)	-0.952	-1.1	-0.595	0.199	0.338	0.241	0.509
4 (0.244)	-0.784	-2.537	-0.63	0.163	0.196	0.172	0.244
5 (-0.021)	-0.642	-2.582	-0.749	0.148	0.005	0.178	-0.021
6 (-0.287)	-0.484	-2.539	-0.953	0.075	-0.102	0.173	-0.287
7 (-0.552)	-0.372	-2.31	-1.031	-0.038	-0.208	-0.084	-0.552
8 (-0.817)	-0.259	-2.226	-1.074	-0.127	-0.296	-0.173	-0.817
9 (-1.082)	-0.167	-2.147	-1.145	-0.195	-0.376	-0.261	-1.082
10 (-1.347)	-0.1	-2.156	-1.356	-0.23	-0.437	-0.253	-1.347
11 (-1.689)	-0.204	-2.592	-1.387	-0.231	-0.395	-0.273	-1.689
12 (-2.22)	-0.169	-2.582	-1.472	-0.222	-0.428	-0.285	-2.22
13 (-2.752)	-0.157	-2.579	-1.525	-0.164	-0.438	-0.288	-2.752
14 (-3.283)	-0.154	-2.578	-1.429	-0.111	-0.442	-0.289	-3.283
15 (-3.814)	-0.153	-2.578	-1.248	-0.171	-0.443	-0.289	-3.814
16 (-4.345)	-0.152	-2.578	-1.103	-0.028	-0.443	-0.289	-4.345
17 (-4.877)	-0.151	-2.577	-1.324	-0.067	-0.444	-0.289	-4.877
18 (-5.408)	-0.15	-2.577	-0.665	-0.367	-0.445	-0.289	-5.408
19 (-6.05)	-2.027	-4.746	1.086	-1.6	-0.442	-0.29	-6.05
20 (-8.676)	0.541	-4.242	1.677	-2.154	-1.344	-0.316	-8.676